

1 **OPTIMIZATION OF THE MEAN FIRST PASSAGE TIME IN**
2 **NEAR-DISK AND ELLIPTICAL DOMAINS IN 2-D WITH SMALL**
3 **ABSORBING TRAPS**

4 SARAJA IYANIWURA*, TONY WONG*, COLIN B. MACDONALD*, AND MICHAEL J.
5 WARD* †

6 **Abstract.** The determination of the mean first passage time (MFPT) for a Brownian particle in
7 a bounded 2-D domain containing small absorbing traps is a fundamental problem with biophysical
8 applications. The average MFPT is the expected capture time assuming a uniform distribution of
9 starting points for the random walk. We develop a hybrid asymptotic-numerical approach to predict
10 optimal configurations of m small stationary circular absorbing traps that minimize the average
11 MFPT in near-disk and elliptical domains. For a general class of near-disk domains, we illustrate
12 through several specific examples how simple, but yet highly accurate, numerical methods can be used
13 to implement the asymptotic theory. From the derivation of a new explicit formula for the Neumann
14 Green's function and its regular part for the ellipse, a numerical approach based on our asymptotic
15 theory is used to investigate how the spatial distribution of the optimal trap locations changes as the
16 aspect ratio of an ellipse of fixed area is varied. The results from the hybrid theory for the ellipse
17 are compared with full PDE numerical results computed from the closest point method [10]. For
18 long and thin ellipses, it is shown that the optimal trap pattern for $m = 2, \dots, 5$ identical traps is
19 collinear along the semi-major axis of the ellipse. For such essentially 1-D patterns, a thin-domain
20 asymptotic analysis is formulated and implemented to accurately predict the optimal locations of
21 collinear trap patterns and the corresponding optimal average MFPT.

22 **1. Introduction.** The concept of first passage time arises in various applications
23 in biology, biochemistry, ecology, physics, and biophysics (see [6], [7], [20], [15] [23],
24 [21], and the references therein). Narrow escape or capture problems are first passage
25 time problems that characterize the expected time it takes for a Brownian “particle”
26 to reach some absorbing set of small measure. These problems are of singular pertur-
27 bation type as they involve two spatial scales: the $\mathcal{O}(1)$ spatial scale of the confining
28 domain and the $\mathcal{O}(\varepsilon)$ asymptotically small scale of the absorbing set. Narrow escape
29 and capture problems arise in various applications, including estimating the time it
30 takes for a receptor to hit a certain target binding site, the time it takes for a diffusing
31 surface-bound molecules to reach a localized signaling region on the cell membrane,
32 or the time it takes for a predator to locate its prey, among others (cf. [1], [2], [4],
33 [3], [9], [16], [24], [19], [15]). A comprehensive overview of the applications of narrow
34 escape and capture problems in cellular biology is given in [8].

35 In this paper, we consider a narrow capture problem that involves determining
36 the MFPT for a Brownian particle, confined in a bounded two-dimensional domain,
37 to reach one of m small stationary circular absorbing traps located inside the domain.
38 The average MFPT for this diffusion process is the expected time for capture given a
39 uniform distribution of starting points for the random walk. In the limit of small trap
40 radius, this narrow capture problem can be analyzed by techniques in strong localized
41 perturbation theory (cf. [26], [27]). For a disk-shaped domain spatial configurations
42 of small absorbing traps that minimize the average MFPT domain were identified
43 in [12]. However, the problem of identifying optimal trap configurations in other
44 geometries is largely open. In this direction, the specific goal of this paper is to
45 develop and implement a hybrid asymptotic-numerical theory to identify optimal trap
46 configurations in near-disk domains and in the ellipse.

47 In § 2, we use a perturbation approach to derive a two-term approximation for

*Dept. of Mathematics, Univ. of British Columbia, Vancouver, B.C., Canada.

†corresponding author, ward@math.ubc.ca

48 the average MFPT in a class of near-disk domains in terms of a boundary deformation
 49 parameter $\sigma \ll 1$. In our analysis, we allow for a smooth, but otherwise arbitrary, star-
 50 shaped perturbation of the unit disk that preserves the domain area. At each order
 51 in σ , an approximate solution is derived for the MFPT that is accurate to all orders
 52 in $\nu \equiv -1/\log \varepsilon$, where $\varepsilon \ll 1$ is the common radius of the m circular absorbing traps
 53 contained in the domain. To leading-order in σ , this small-trap singular perturbation
 54 analysis is formulated in the unit disk and leads to a linear algebraic system for the
 55 leading-order average MFPT involving the Neumann Green's matrix. At order $\mathcal{O}(\sigma)$,
 56 a further linear algebraic system that sums all logarithmic terms in ν is derived that
 57 involves the Neumann Green's matrix and certain weighted integrals of the boundary
 58 profile characterizing the domain perturbation. In § 3, we show how to numerically
 59 implement this asymptotic theory by using the analytical expression for the Neumann
 60 Green's function for the unit disk together with the trapezoidal rule to compute certain
 61 weighted integrals of the boundary profile with high precision. From this numerical
 62 implementation of our asymptotic theory, and combined with either a simple gradient
 63 descent procedure or a particle swarming approach [11], we can numerically identify
 64 optimal trap configurations that minimize the average MFPT in near-disk domains.
 65 In § 3.1, we illustrate our hybrid asymptotic-numerical framework by determining
 66 some optimal trap configurations in various specific near-disk domains.

67 For a general 2-D domain containing small absorbing traps, a singular pertur-
 68 bation analysis in the limit of small trap radii, related to that in [15], [4], [12], and
 69 [26], shows that the average MFPT is closely approximated by the solution to a linear
 70 algebraic system involving the Neumann Green's matrix. The challenge in implement-
 71 ing this analytical theory is that, for an arbitrary 2-D domain, a full PDE numerical
 72 solution of the Neumann Green's function and its regular part is typically required to
 73 calculate this matrix. However, for an elliptical domain, in (4.5) and (4.6) below, we
 74 provide a new explicit representation of this Neumann Green's function and its regular
 75 part. These explicit formulae allow for a rapid numerical evaluation of the Neumann
 76 Green's interaction matrix for a given spatial distribution of the centers of the circular
 77 traps in the ellipse. The linear algebraic system determining the average MFPT is
 78 then coupled to a gradient descent numerical procedure in order to readily identify
 79 optimal trap configurations that minimize the average MFPT in an ellipse. Although,
 80 a similar formula for the Neumann Green's function has been derived previously for a
 81 rectangular domain (cf. [17], [18], [14]), and an explicit and simple formula exists for
 82 the disk [12], to our knowledge there has been no prior derivation of a rapidly con-
 83 verging infinite series representation for the Neumann Green's function in an ellipse.
 84 The derivation of this Neumann Green's function using elliptic cylindrical coordinates
 85 is deferred until § 5.

86 With this explicit approach to determine the Neumann Green's matrix, in § 4
 87 we develop a hybrid asymptotic-numerical framework to approximate optimal trap
 88 configurations that minimize the average MFPT in an ellipse of a fixed area. In § 4.1
 89 we implement our hybrid method to investigate how the optimal trap patterns change
 90 as the aspect ratio of the ellipse is varied. The results from the hybrid theory for the
 91 ellipse are favorably compared with full PDE numerical results computed from a
 92 computationally intensive numerical procedure of using the closest point method [10]
 93 to compute the average MFPT and a particle swarming approach [11] to numerically
 94 identify the optimum trap configuration. As the ellipse becomes thinner, our hybrid
 95 theory shows that the optimal trap pattern for $m = 2, \dots, 5$ identical traps becomes
 96 collinear along the semi-major axis of the ellipse. In the limit of a long and thin
 97 ellipse, in § 4.2 a thin-domain asymptotic analysis is formulated and implemented

98 to accurately predict the optimal locations of collinear trap configurations and the
99 corresponding optimal average MFPT.

100 In § 6, we show that the optimal trap configurations that minimize the average
101 MFPT also correspond to trap patterns that maximize the coefficient of order $\mathcal{O}(\nu^2)$ in
102 the asymptotic expansion of the fundamental Neumann eigenvalue of the Laplacian in
103 the perforated domain. This fundamental eigenvalue characterizes the rate of capture
104 of the Brownian particle by the traps. Eigenvalue optimization problems for the
105 fundamental Neumann eigenvalue in a domain with small absorbing traps have been
106 studied in [12] for the unit disk. The results herein extend this previous analysis to
107 the ellipse and to near-disk domains.

108 **2. Asymptotics of the MFPT in Near-Disk Domains.** We derive an as-
109 ymptotic approximation for the MFPT for a class of near-disk 2-D domains that are
110 defined in polar coordinates by

$$111 \quad (2.1) \quad \Omega_\sigma = \left\{ (r, \theta) \mid 0 < r \leq 1 + \sigma h(\theta), 0 \leq \theta \leq 2\pi \right\},$$

112 where the boundary profile, $h(\theta)$, is assumed to be an $\mathcal{O}(1)$, C^∞ smooth 2π periodic
113 function with $\int_0^{2\pi} h(\theta) d\theta = 0$. Observe that $\Omega_\sigma \rightarrow \Omega$ as $\sigma \rightarrow 0$, where Ω is the unit
114 disk. Since $\int_0^{2\pi} h(\theta) d\theta = 0$, the domain area $|\Omega_\sigma|$ for $\sigma \ll 1$ is $|\Omega_\sigma| = \pi + \mathcal{O}(\sigma^2)$.

115 Inside the perturbed disk Ω_σ , we assume that there are m circular traps of a
116 common radius $\varepsilon \ll 1$ that are centered at arbitrary locations $\mathbf{x}_1, \dots, \mathbf{x}_m$ with $|\mathbf{x}_i -$
117 $\mathbf{x}_j| = \mathcal{O}(1)$ and $\text{dist}(\partial\Omega_\sigma, \mathbf{x}_j) = \mathcal{O}(1)$ as $\varepsilon \rightarrow 0$. The j -th trap, centered at some
118 $\mathbf{x}_j \in \Omega_\sigma$, is labelled by $\Omega_{\varepsilon j} = \{\mathbf{x} : |\mathbf{x} - \mathbf{x}_j| \leq \varepsilon\}$. The near-disk domain with the
119 union of the trap regions deleted is denoted by $\bar{\Omega}_\sigma$. In $\bar{\Omega}_\sigma$, it is well-known that the
120 mean first passage time (MFPT) for a Brownian particle starting at a point $\mathbf{x} \in \bar{\Omega}_\sigma$
121 to be absorbed by one of the traps satisfies (cf. [20])

$$122 \quad (2.2) \quad \begin{aligned} D \Delta u &= -1, & \mathbf{x} \in \bar{\Omega}_\sigma; & \quad \bar{\Omega}_\sigma \equiv \Omega_\sigma \setminus \cup_{j=1}^m \Omega_{\varepsilon j}, \\ \partial_n u &= 0, & \mathbf{x} \in \partial\Omega_\sigma; & \quad u = 0, \quad \mathbf{x} \in \partial\Omega_{\varepsilon j}, \quad j = 1, \dots, m. \end{aligned}$$

123 In terms of polar coordinates, the Neumann boundary condition in (2.2) becomes

$$124 \quad (2.3) \quad u_r - \frac{\sigma h_\theta}{(1 + \sigma h)^2} u_\theta = 0 \quad \text{on} \quad r = 1 + \sigma h(\theta).$$

125 For an arbitrary arrangement $\{\mathbf{x}_1, \dots, \mathbf{x}_m\}$ of the centers of the traps, and for
126 $\sigma \rightarrow 0$ and $\varepsilon \rightarrow 0$, we will derive a reduced problem consisting of two linear algebraic
127 systems that provide an asymptotic approximation to the MFPT that has an error
128 $\mathcal{O}(\sigma^2, \varepsilon^2)$. These linear algebraic systems involve the Neumann Green's matrix and
129 certain weighted integrals of the boundary profile $h(\theta)$.

130 To analyze (2.2), we use a regular perturbation series to approximate (2.2) for
131 the near-disk domain to problems involving a unit disk. We expand the MFPT u as

$$132 \quad (2.4) \quad u = u_0 + \sigma u_1 + \dots,$$

133 and substitute it into (2.2) and (2.3). This yields the leading-order problem

$$134 \quad (2.5) \quad \begin{aligned} D \Delta u_0 &= -1, & \mathbf{x} \in \bar{\Omega}; & \quad \bar{\Omega} \equiv \Omega \setminus \cup_{j=1}^m \Omega_{\varepsilon j}, \\ \partial_n u_0 &= 0, & \text{on} \quad r = 1; & \quad u_0 = 0, \quad \mathbf{x} \in \partial\Omega_{\varepsilon j}, \quad j = 1, \dots, m, \end{aligned}$$

135 together with the following problem for the next order correction u_1 :

$$136 \quad (2.6) \quad \begin{aligned} \Delta u_1 &= 0, \quad \mathbf{x} \in \bar{\Omega}; & \partial_r u_1 &= -h u_{0rr} + h_\theta u_{0\theta}, \quad \text{on } r = 1; \\ u_1 &= 0, \quad \mathbf{x} \in \partial\Omega_{\varepsilon_j}, & j &= 1, \dots, m. \end{aligned}$$

137 Observe that (2.5) and (2.6) are formulated on the unit disk and not on the perturbed
138 disk. Assuming $\varepsilon^2 \ll \sigma$, we use (2.4) and $|\Omega_\sigma| = |\Omega| + \mathcal{O}(\sigma^2)$ to derive an expansion
139 for the average MFPT, defined by $\bar{u} \equiv \frac{1}{|\Omega_\sigma|} \int_{\Omega_\sigma} u \, d\mathbf{x}$, in the form

$$140 \quad (2.7) \quad \bar{u} = \frac{1}{|\Omega|} \int_{\Omega} u_0 \, d\mathbf{x} + \sigma \left[\frac{1}{|\Omega|} \int_{\Omega} u_1 \, d\mathbf{x} + \frac{1}{|\Omega|} \int_0^{2\pi} h(\theta) u_0|_{r=1} \, d\theta \right] + \mathcal{O}(\sigma^2, \varepsilon^2),$$

141 where $|\Omega| = \pi$ and $u_0|_{r=1}$ is the leading-order solution u_0 evaluated on $r = 1$.

142 Since the asymptotic calculation of the leading-order solution u_0 by the method
143 of matched asymptotic expansions in the limit $\varepsilon \rightarrow 0$ of small trap radius was done
144 previously in [4] (see also [15] and [26]), we only briefly summarize the analysis here.
145 In the inner region near the j -th trap, we define the inner variables $\mathbf{y} = \varepsilon^{-1}(\mathbf{x} - \mathbf{x}_j)$
146 and $u_0(\mathbf{x}) = v_j(\varepsilon\mathbf{y} + \mathbf{x}_j)$ with $\rho = |\mathbf{y}|$, for $j = 1, \dots, m$. Upon writing (2.5) in terms
147 of these inner variables, we have for $\varepsilon \rightarrow 0$ and for each $j = 1, \dots, m$ that

$$148 \quad (2.8) \quad \Delta_\rho v_j = 0, \quad \rho > 1; \quad v_j = 0, \quad \text{on } \rho = 1,$$

149 where $\Delta_\rho \equiv \partial_{\rho\rho} + \rho^{-1}\partial_\rho$. This admits the radially symmetric solution $v_j = A_j \log \rho$,
150 where A_j is an unknown constant. From an asymptotic matching of the inner and
151 outer solutions we obtain the required singularity condition for the outer solution u_0
152 as $\mathbf{x} \rightarrow \mathbf{x}_j$ for $j = 1, \dots, m$. In this way, we obtain that u_0 satisfies

$$153 \quad (2.9a) \quad \Delta u_0 = -1/D, \quad \mathbf{x} \in \Omega \setminus \{\mathbf{x}_1, \dots, \mathbf{x}_m\}; \quad \partial_r u_0 = 0, \quad \mathbf{x} \in \partial\Omega;$$

$$154 \quad (2.9b) \quad u_0 \sim A_j \log |\mathbf{x} - \mathbf{x}_j| + A_j/\nu \quad \text{as } \mathbf{x} \rightarrow \mathbf{x}_j, \quad j = 1, \dots, m,$$

156 where $\nu \equiv -1/\log \varepsilon$. In terms of the Delta distribution, (2.9) implies that

$$157 \quad (2.10) \quad \Delta u_0 = -\frac{1}{D} + 2\pi \sum_{j=1}^m A_j \delta(\mathbf{x} - \mathbf{x}_j), \quad \mathbf{x} \in \Omega; \quad \partial_r u_0 = 0, \quad \mathbf{x} \in \partial\Omega.$$

158 By applying the divergence theorem to (2.10) over the unit disk we obtain that
159 $\sum_{j=1}^m A_j = |\Omega|/(2\pi D)$. The solution to (2.10) is represented as

$$160 \quad (2.11) \quad u_0 = -2\pi \sum_{k=1}^m A_k G(\mathbf{x}; \mathbf{x}_k) + \bar{u}_0; \quad \bar{u}_0 = \frac{1}{|\Omega|} \int_{\Omega} u_0 \, d\mathbf{x},$$

162 where $G(\mathbf{x}; \mathbf{x}_j)$ is the Neumann Green's function for the unit disk, which satisfies

$$163 \quad (2.12a) \quad \Delta G = \frac{1}{|\Omega|} - \delta(\mathbf{x} - \mathbf{x}_j), \quad \mathbf{x} \in \Omega; \quad \partial_n G = 0, \quad \mathbf{x} \in \partial\Omega; \quad \int_{\Omega} G \, d\mathbf{x} = 0,$$

$$164 \quad (2.12b) \quad G \sim -\frac{1}{2\pi} \log |\mathbf{x} - \mathbf{x}_j| + R_j + \nabla_{\mathbf{x}} R_j \cdot (\mathbf{x} - \mathbf{x}_j) \quad \text{as } \mathbf{x} \rightarrow \mathbf{x}_j.$$

166 Here, $R_j \equiv R(\mathbf{x}_j)$ is the regular part of the Green's function at $\mathbf{x} = \mathbf{x}_j$. Expanding
167 (2.11) as $\mathbf{x} \rightarrow \mathbf{x}_j$, and using the singularity behaviour of $G(\mathbf{x}; \mathbf{x}_j)$ given in (2.12b),
168 together with the far-field behavior (2.9b) for u_0 , we obtain the matching condition:

$$169 \quad (2.13) \quad -2\pi A_j R_j - 2\pi \sum_{i \neq j}^m A_i G(\mathbf{x}_j; \mathbf{x}_i) + \bar{u}_0 \sim A_j/\nu, \quad \text{for } j = 1, \dots, m.$$

170 This yields a linear algebraic system for \bar{u}_0 and $\mathcal{A} \equiv (A_1, \dots, A_m)^T$, given by

$$171 \quad (2.14) \quad (I + 2\pi\nu\mathcal{G})\mathcal{A} = \nu\bar{u}_0\mathbf{e}, \quad \mathbf{e}^T\mathcal{A} = \frac{|\Omega|}{2\pi D}.$$

173 Here, $\mathbf{e} \equiv (1, \dots, 1)^T$, $\nu = -1/\log \varepsilon$, I is the $m \times m$ identity matrix, and \mathcal{G} is the
174 symmetric Green's matrix with matrix entries given by

$$175 \quad (2.15) \quad (\mathcal{G})_{jj} = R_j \text{ for } i = j \quad \text{and} \quad (\mathcal{G})_{ij} = (\mathcal{G})_{ji} = G(\mathbf{x}_i; \mathbf{x}_j) \text{ for } i \neq j.$$

177 We left-multiply the equation for \mathcal{A} in (2.14) by \mathbf{e}^T , which isolates \bar{u}_0 . By using this
178 expression in (2.14), and defining the matrix E by $E = \mathbf{e}\mathbf{e}^T/m$, we get

$$179 \quad (2.16) \quad \left[I + 2\pi\nu(I - E)\mathcal{G} \right] \mathcal{A} = \frac{|\Omega|}{2\pi Dm} \mathbf{e}, \quad \text{and} \quad \bar{u}_0 = \frac{|\Omega|}{2\pi D\nu m} + \frac{2\pi}{m} \mathbf{e}^T \mathcal{G} \mathcal{A}.$$

180 *Remark 2.1.* The result (2.16) effectively sums all the logarithmic terms in powers
181 of $\nu = -1/\log \varepsilon$. To estimate the error with this approximation with regards to the
182 leading-order in σ problem (2.5), we calculate using (2.11) the refined local behavior

$$183 \quad (2.17) \quad u_0 \sim -2\pi \left(A_j R_j + \sum_{i \neq j}^m A_i G(\mathbf{x}_j; \mathbf{x}_i) \right) + \bar{u}_0 + \mathbf{f}_j \cdot (\mathbf{x} - \mathbf{x}_j), \quad \text{as } \mathbf{x} \rightarrow \mathbf{x}_j,$$

184 where $\mathbf{f}_j \equiv -2\pi \left(A_j \nabla_{\mathbf{x}} R_j + \sum_{i \neq j}^m A_i \nabla_{\mathbf{x}} G(\mathbf{x}; \mathbf{x}_i)|_{\mathbf{x}=\mathbf{x}_j} \right)$. To account for this gradient
185 term, near the j -th trap we must modify the inner expansion as $v_j \sim A_j \log \rho + \varepsilon v_{j1}$.
186 Here $\Delta_{\mathbf{y}} v_{j1} = 0$ in $|\mathbf{y}| \geq 1$, with $v_{j1} = 0$ on $|\mathbf{y}| = 1$ and $v_{j1} \sim \mathbf{f}_j \cdot \mathbf{y}$ as $|\mathbf{y}| \rightarrow \infty$. The
187 solution is $v_{j1} = \mathbf{f}_j \cdot (\mathbf{y} - \mathbf{y}/|\mathbf{y}|^2)$. The far field behavior for v_{j1} implies that in the
188 outer region we must have that $u \sim u_0 + \varepsilon^2 w_0 + \dots$, where $w_0 \sim -\mathbf{f}_j \cdot (\mathbf{x} - \mathbf{x}_j)/|\mathbf{x} - \mathbf{x}_j|^2$
189 as $\mathbf{x} \rightarrow \mathbf{x}_j$. This shows that the ε -error estimate for u_0 is $\mathcal{O}(\varepsilon^2)$, as claimed in (2.7).

190 Next, we study the $\mathcal{O}(\sigma)$ problem for u_1 given in (2.6). We construct an inner
191 region near each of the traps by introducing the inner variables $\mathbf{y} = \varepsilon^{-1}(\mathbf{x} - \mathbf{x}_j)$
192 and $u_1(\mathbf{x}) = V_j(\varepsilon\mathbf{y} + \mathbf{x}_j)$ with $\rho = |\mathbf{y}|$. From (2.6), this yields the same leading-
193 order inner problem (2.8) with v_j replaced by V_j . The radially symmetric solution is
194 $V_j = B_j \log \rho$, where B_j is a constant to be found. By matching this far-field behavior
195 of the inner solution to the outer solution we obtain the singularity behavior for u_1
196 as $\mathbf{x} \rightarrow \mathbf{x}_j$ for $j = 1, \dots, m$. In this way, we find from (2.6) that u_1 satisfies

$$197 \quad (2.18a) \quad \Delta u_1 = 0, \quad \mathbf{x} \in \Omega \setminus \{\mathbf{x}_1, \dots, \mathbf{x}_m\}; \quad \partial_r u_1 = F(\theta), \quad \text{on } r = 1;$$

$$198 \quad (2.18b) \quad u_1 \sim B_j \log |\mathbf{x} - \mathbf{x}_j| + B_j/\nu \quad \text{as } \mathbf{x} \rightarrow \mathbf{x}_j \quad j = 1, \dots, m,$$

200 where $\nu = -1/\log \varepsilon$ and $F(\theta)$ is defined by

$$201 \quad (2.18c) \quad F(\theta) \equiv -h u_{0rr}|_{r=1} + h_\theta u_{0\theta}|_{r=1} = (h u_{0\theta})_\theta + \frac{h}{D}.$$

202 In deriving (2.18c) we used $u_{0rr} = -u_{0\theta\theta} + 1/D$ at $r = 1$, as obtained from (2.5).

203 Next, we introduce the Dirac distribution and write the problem (2.18) for u_1 as

$$204 \quad (2.19) \quad \Delta u_1 = 2\pi \sum_{i=1}^m B_i \delta(\mathbf{x} - \mathbf{x}_i), \quad \mathbf{x} \in \Omega; \quad u_{1r} = F(\theta), \quad \text{on } r = 1.$$

205

206 Since $\int_0^{2\pi} F(\theta) d\theta = 0$, the divergence theorem yields $\sum_{j=1}^m B_j = 0$. We decompose

$$207 \quad (2.20) \quad u_1 = -2\pi \sum_{i=1}^m B_i G(\mathbf{x}; \mathbf{x}_i) + u_{1p} + \bar{u}_1,$$

208 where \bar{u}_1 is the unknown average of u_1 over the unit disk, and $G(\mathbf{x}; \mathbf{x}_i)$ is the Neumann
209 Green's function satisfying (2.12). Here, u_{1p} is taken to be the unique solution to

$$210 \quad (2.21) \quad \Delta u_{1p} = 0, \quad \mathbf{x} \in \Omega; \quad \partial_r u_{1p} = F(\theta) \quad \text{on} \quad r = 1; \quad \int_{\Omega} u_{1p} d\mathbf{x} = 0.$$

212 Next, by expanding (2.20) as $\mathbf{x} \rightarrow \mathbf{x}_j$, we use the singularity behaviour of $G(\mathbf{x}; \mathbf{x}_j)$
213 as given in (2.12b) to obtain the local behavior of u_1 as $\mathbf{x} \rightarrow \mathbf{x}_j$, for each $j = 1, \dots, m$.
214 The asymptotic matching condition is that this behavior must agree with that given
215 in (2.18b). In this way, we obtain a linear algebraic system for the constant \bar{u}_1 and
216 the vector $\mathbf{B} = (B_1, \dots, B_m)^T$, which is given in matrix form by

$$217 \quad (2.22) \quad (I + 2\pi\nu\mathcal{G})\mathbf{B} = \nu\bar{u}_1\mathbf{e} + \nu\mathbf{u}_{1p}, \quad \mathbf{e}^T\mathbf{B} = 0.$$

218 Here, I is the identity, $\mathbf{e} = (1, \dots, 1)^T$, and $\mathbf{u}_{1p} = (u_{1p}(\mathbf{x}_1), \dots, u_{1p}(\mathbf{x}_m))^T$. Next,
219 we left multiply the equation for \mathbf{B} by \mathbf{e}^T . This determines \bar{u}_1 , which is then re-
220 substituted into (2.22) to obtain the uncoupled problem

$$221 \quad (2.23) \quad \left[I + 2\pi\nu(I - E)\mathcal{G} \right] \mathbf{B} = \nu(I - E)\mathbf{u}_{1p}, \quad \text{and} \quad \bar{u}_1 = -\frac{1}{m}\mathbf{e}^T\mathbf{u}_{1p} + \frac{2\pi}{m}\mathbf{e}^T\mathcal{G}\mathbf{B},$$

222 where $E \equiv \mathbf{e}\mathbf{e}^T/m$. Since $\mathbf{e}^T(I - E) = 0$, we observe from (2.23) that $\mathbf{e}^T\mathbf{B} = 0$, as
223 required. Equation (2.23) gives a linear system for the $\mathcal{O}(\sigma)$ average MFPT \bar{u}_1 in
224 terms of the Neumann Green's matrix \mathcal{G} , and the vector \mathbf{u}_{1p} .

225 To determine $u_{1p}(\mathbf{x}_j)$, we use Green's second identity on (2.21) and (2.12) to
226 obtain a line integral over the boundary $\mathbf{x} \in \partial\Omega$ of the unit disk. Then, by using
227 (2.18c) for $F(\theta)$, integrating by parts and using 2π periodicity we get

$$228 \quad (2.24) \quad u_{1p}(\mathbf{x}_j) = \int_0^{2\pi} G(\mathbf{x}; \mathbf{x}_j) F(\theta) d\theta = \int_0^{2\pi} G(\mathbf{x}; \mathbf{x}_j) \frac{h(\theta)}{D} d\theta - \int_0^{2\pi} h(\theta) u_{0\theta} \partial_\theta G(\mathbf{x}; \mathbf{x}_j) d\theta.$$

229 Then, by setting (2.11) for u_0 into (2.24), we obtain in terms of the A_k of (2.16) that

$$230 \quad (2.25a) \quad u_{1p}(\mathbf{x}_j) = \frac{1}{D} \int_0^{2\pi} G(\mathbf{x}; \mathbf{x}_j) h(\theta) d\theta + 2\pi \sum_{k=1}^m A_k J_{jk}.$$

231 Here, J_{jk} is defined by the following boundary integral with $\mathbf{x} = (\cos(\theta), \sin(\theta))^T$:

$$232 \quad (2.25b) \quad J_{jk} \equiv \int_0^{2\pi} h(\theta) (\partial_\theta G(\mathbf{x}; \mathbf{x}_j)) (\partial_\theta G(\mathbf{x}; \mathbf{x}_k)) d\theta.$$

233 From a numerical evaluation of the boundary integrals in (2.25), we can calculate
234 $\mathbf{u}_{1p} = (u_{1p}(\mathbf{x}_1), \dots, u_{1p}(\mathbf{x}_m))^T$, which specifies the right-hand side of the linear system
235 (2.23) for \mathbf{B} . After determining \mathbf{B} , we obtain \bar{u}_1 from the second relation in (2.23).
236 Finally, by substituting (2.11) for u_0 into (2.7), and recalling that $\int_0^{2\pi} h(\theta) d\theta = 0$, we
237 obtain a two-term expansion for the average MFPT given by

$$238 \quad (2.26) \quad \bar{u} \sim \bar{u}_0 + \sigma \left(\bar{u}_1 - 2 \sum_{k=1}^m A_k \int_0^{2\pi} G(\mathbf{x}; \mathbf{x}_k) h(\theta) d\theta \right).$$

239 Here, \bar{u}_0 and \bar{u}_1 are determined from (2.16).

3. Optimizing Trap Configurations for the MFPT in the Near-Disk.

To numerically evaluate the boundary integrals in (2.25) and (2.26), we need explicit formulae for $G(\mathbf{x}; \mathbf{x}_j)$ and $\partial_\theta G(\mathbf{x}; \mathbf{x}_j)$ on the boundary of the unit disk where $\mathbf{x} = (\cos \theta, \sin \theta)^T$. For the unit disk, we obtain from equation (4.3) of [12] that

(3.1a)

$$G(\mathbf{x}; \mathbf{x}_j) = -\frac{1}{2\pi} \log |\mathbf{x} - \mathbf{x}_j| - \frac{1}{4\pi} \log (|\mathbf{x}|^2 |\mathbf{x}_j|^2 + 1 - 2\mathbf{x} \cdot \mathbf{x}_j) + \frac{(|\mathbf{x}|^2 + |\mathbf{x}_j|^2)}{4\pi} - \frac{3}{8\pi},$$

$$R(\mathbf{x}_j; \mathbf{x}_j) = -\frac{1}{2\pi} \log (1 - |\mathbf{x}_j|^2) + \frac{|\mathbf{x}_j|^2}{2\pi} - \frac{3}{8\pi}.$$

For an arbitrary configuration $\{\mathbf{x}_1, \dots, \mathbf{x}_m\}$ of traps, these expressions can be used to evaluate the Neumann Green's matrix \mathcal{G} of (2.15) as needed in (2.16) and (2.23).

Next, by setting $\mathbf{x} = (\cos \theta, \sin \theta)^T$ we can evaluate $G(\mathbf{x}; \mathbf{x}_j)$ on $\partial\Omega$, and then calculate its tangential boundary derivative $\partial_\theta G(\mathbf{x}; \mathbf{x}_j)$. By using (3.1a), we obtain

$$G(\mathbf{x}; \mathbf{x}_j) = -\frac{1}{2\pi} \log (1 + r_j^2 - 2r_j \cos(\theta - \theta_j)) + \frac{1}{4\pi} (1 + r_j^2) - \frac{3}{8\pi},$$

$$\partial_\theta G(\mathbf{x}; \mathbf{x}_j) = -\frac{r_j}{\pi} \frac{\sin(\theta - \theta_j)}{[r_j^2 + 1 - 2r_j \cos(\theta - \theta_j)]},$$

where $r_j \equiv |\mathbf{x}_j|$ and $\mathbf{x}_j = r_j(\cos \theta_j, \sin \theta_j)^T$. Then, since $\int_0^{2\pi} h(\theta) d\theta = 0$, we can write the two boundary integrals appearing in (2.25) and (2.26) explicitly as

$$\int_0^{2\pi} G(\mathbf{x}; \mathbf{x}_j) h(\theta) d\theta = -\frac{1}{2\pi} \int_0^{2\pi} h(\theta) \log (1 + r_j^2 - 2r_j \cos(\theta - \theta_j)) d\theta,$$

$$J_{jk} = \frac{r_j r_k}{\pi^2} \int_0^{2\pi} \frac{h(\theta) \sin(\theta - \theta_j) \sin(\theta - \theta_k)}{[r_j^2 + 1 - 2r_j \cos(\theta - \theta_j)] [r_k^2 + 1 - 2r_k \cos(\theta - \theta_k)]} d\theta.$$

Although for an arbitrary $h(\theta)$ the integrals in (3.3) cannot be evaluated in closed form, they can be computed to a high degree of accuracy with relatively few grid points using the trapezoidal rule since this quadrature rule is exponentially convergent for C^∞ smooth periodic functions [25]. When $|x_j| < 1$, the logarithmic singularities of the axis of integration for J_{jk} in (3.3) are mild and pose no particular problem. In this way, we can numerically calculate the two-term expansion (2.26) for the average MFPT with high precision.

Then, to determine the optimal trap configuration we can either use the particle swarming approach [11], or the ODE relaxation dynamics scheme

$$\frac{d\mathbf{z}}{dt} = -\nabla_{\mathbf{z}} \bar{u}, \quad \text{where } \mathbf{z} \equiv (x_1, y_1, \dots, x_m, y_m)^T,$$

and \bar{u} is given in (2.26). Starting from an admissible initial state $\mathbf{z}|_{t=0}$, where $\mathbf{x}_j = (x_j, y_j) \in \Omega_0$ at $t = 0$ for $j = 1, \dots, m$, the gradient flow dynamics (3.4) converges to a local minimum of \bar{u} . Because of our high precision in calculating \bar{u} , a centered difference scheme with mesh spacing 10^{-4} was used to estimate the gradient in (3.4).

3.1. Examples of the Theory. We first set $\sigma = 0.1$ and consider the boundary profile $h(\theta) = \cos(N\theta)$, where N is a positive integer representing the number of boundary folds. In [10], an explicit two-term expansion for the average MFPT \bar{u} was derived for the special case where m traps are equidistantly spaced on a ring of radius

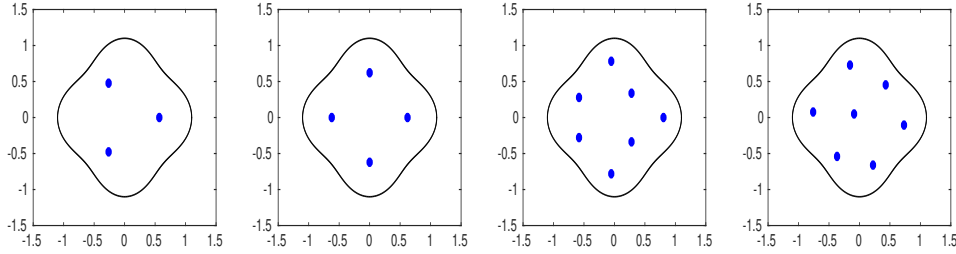


FIG. 1. *Optimal trap patterns for $D = 1$ in a near-disk domain with boundary $r = 1 + \sigma \cos(4\theta)$, with $\sigma = 0.1$, that contains m traps of a common radius $\varepsilon = 0.05$. Computed from minimizing (2.26) using the ODE relaxation scheme (3.4). Left: $m = 3$, $\bar{u} \approx 0.2962$. Inter-trap computed distances are 0.9588, 0.9588, and 0.9540. This result is close to the full PDE simulation results of Fig. 2. Left middle: $m = 4$, $\bar{u} \approx 0.1927$. This is a ring pattern of traps with ring radius $r_c \approx 0.6215$. Right Middle: $m = 7$, $\bar{u} \approx 0.0925$. Right: $m = 7$, $\bar{u} \approx 0.0912$. The two patterns for $m = 7$ give nearly the same values for \bar{u} , with the rightmost pattern giving a slightly lower value.*

277 r_c , concentric within the unperturbed disk. For such a ring pattern, in Proposition 1
 278 of [10] it was proved that when $N/m \notin \mathbb{Z}^+$, then $\bar{u} \sim \bar{u}_0 + \mathcal{O}(\sigma^2)$, as the correction
 279 at order $\mathcal{O}(\sigma)$ vanishes identically. Therefore, in order to determine the optimal trap
 280 pattern when $N/m \notin \mathbb{Z}^+$ we must consider arbitrary trap configurations, and not just
 281 ring patterns of traps. By minimizing (2.26) using the ODE relaxation scheme (3.4),
 282 in the left panel of Fig. 1 we show our asymptotic prediction for the optimal trap
 283 configuration for $N = 4$ folds and $m = 3$ traps of a common radius $\varepsilon = 0.05$. The
 284 optimal pattern is not of ring-type. The corresponding results computed from the
 285 closest point method of [10], shown in Fig. 2, are very close to the asymptotic result.

286 In the left-middle panel of Fig. 1, we show the optimal trap pattern computed
 287 from our asymptotic theory (2.26) and (3.4) for the boundary profile $h(\theta) = \cos(4\theta)$
 288 with $m = 4$ traps and $\sigma = 0.1$. The optimal pattern is now a ring pattern of traps. In
 289 this case, as predicted by Proposition 1 of [10], the optimal pattern has traps on the
 290 rays through the origin that coincide with the maxima of the domain boundary. By
 291 applying Proposition 2 of [10], the optimal perturbed ring radius has the expansion
 292 $r_{c,opt} \sim 0.5985 + 0.1985\sigma$. When $\sigma = 0.1$, this gives $r_{c,opt} \approx 0.6184$, and compares
 293 well with the value $r_c \approx 0.6215$ calculated from (2.26) and (3.4).

294 In the two rightmost panels of Fig. 1, we show for $h(\theta) = \cos(4\theta)$ and $\sigma = 0.1$,
 295 that there are two seven-trap patterns that give local minima for the average MFPT
 296 \bar{u}_0 . The minimum values of \bar{u}_0 for these patterns are very similar.

297 Next, we construct a boundary profile with a localized protrusion, or bulge, near
 298 $\theta = 0$. To this end, we define $f(\theta) \equiv -1 + \beta e^{-\chi \sin^2(\theta/2)}$. By using the Taylor
 299 expansion of e^z , combined with a simple identity for $\int_0^{2\pi} \sin^{2n}(\psi) d\psi$, we conclude
 300 that $\int_0^{2\pi} f(\theta) d\theta = 0$ when β is related to χ by
 (3.5)

$$301 \quad \frac{1}{\beta} = \frac{1}{2\pi} \int_0^{2\pi} e^{-\chi \sin^2(\theta/2)} d\theta = \sum_{n=0}^{\infty} \frac{(-1)^n \chi^n}{2\pi n!} \int_0^{2\pi} \sin^{2n} \left(\frac{\theta}{2} \right) d\theta = \sum_{n=0}^{\infty} (-1)^n \frac{\chi^n (2n)!}{4^n (n!)^3}.$$

302 As χ increases, the boundary deformation becomes increasingly localized near $\theta = 0$.

303 For $\chi = 10$, for which $\beta = 5.4484$, in Fig. 3 we show optimal trap patterns for
 304 $m = 3$ and $m = 4$ traps for both an outward domain bulge, where $r = 1 + \sigma f(\theta)$, and
 305 an inward domain bulge, where $r = 1 - \sigma f(\theta)$, with $\sigma = 0.05$. For the three-trap case,
 306 by comparing the two leftmost plots in Fig. 3, we observe that an inward domain bulge

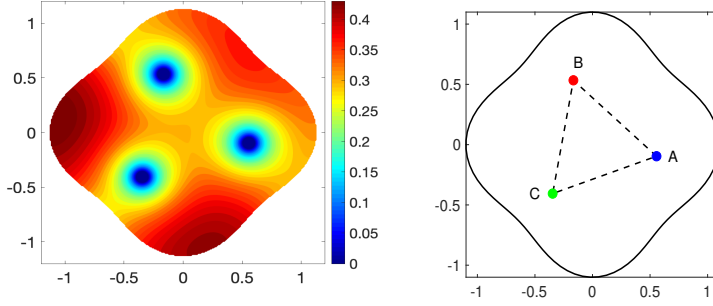


FIG. 2. Optimizing a three-trap pattern, with a common trap radius $\varepsilon = 0.05$, in a four-fold star-shaped domain (4 -star) with boundary profile $h(\theta) = \cos(4\theta)$ and $\sigma = 0.1$. Left panel: contour plot of the optimal PDE solution computed with closest point method. Right panel: optimal traps locations in the 4 -star domain with computed side-lengths: $\mathbf{AB} \approx 0.9581$, $\mathbf{BC} \approx 0.9569$, and $\mathbf{CA} \approx 0.9541$. All of the computed interior angles are $\pi/3 \pm \delta$, where $|\delta| \leq 0.0015$.

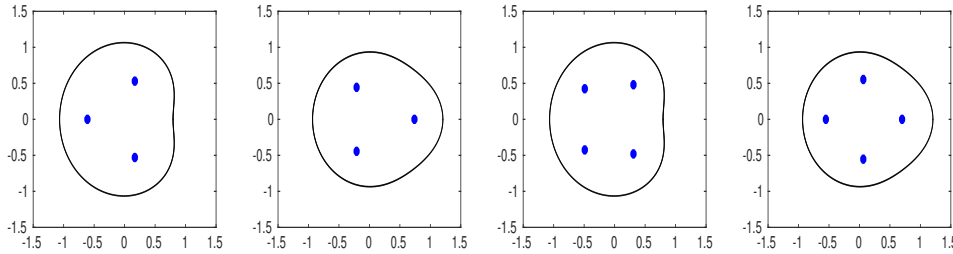


FIG. 3. Optimal trap patterns for $D = 1$ with m traps each of radius $\varepsilon = 0.05$ in a near-disk domain with boundary $r = 1 \pm \sigma f(\theta)$, where $\sigma = 0.05$ and $f(\theta) = -1 + \beta e^{-10 \sin^2(\theta/2)}$, with $\beta = 5.4484$. Computed from minimizing (2.26) using the ODE relaxation scheme (3.4). Left: $m = 3$ and inward domain bulge $r = 1 - \sigma f(\theta)$. Centroid of trap pattern is at $(-0.0886, 0.0)$ and $\bar{u} \approx 0.2842$. Left Middle: $m = 3$ and outward bulge $r = 1 + \sigma f(\theta)$. Centroid is at $(0.1061, 0.0)$, and $\bar{u} \approx 0.2825$. Right Middle: $m = 4$ and inward bulge $r = 1 - \sigma f(\theta)$, $\bar{u} \approx 0.1918$. Right: $m = 4$ and outward bulge $r = 1 + \sigma f(\theta)$, $\bar{u} \approx 0.1916$.

307 will displace the trap locations to the left, as expected intuitively. Alternatively, for
 308 an outward bulge, the location of the optimal trap on the line of symmetry becomes
 309 closer to the domain protrusion. An intuitive, but as we will see below in Fig. 4, naïve
 310 interpretation of the qualitative effect of this domain bulge is that it acts to confine
 311 or pin a Brownian particle in this region, and so in order to reduce the mean capture
 312 time of such a pinned particle, the best location for a trap is to move closer to the
 313 region of protrusion. For the case of four traps, a similar qualitative comparison of
 314 the optimal trap configuration for an inward and outward domain bulge is seen in the
 315 two rightmost plots in Fig. 3.

316 In Fig. 4, we show optimal trap patterns from our hybrid theory for $3 \leq m \leq 5$
 317 circular traps of radius $\varepsilon = 0.05$ in a domain with boundary profile $r = 1 + \sigma h(\theta)$,
 318 where $h(\theta) = \cos(3\theta) - \cos(\theta) - \cos(2\theta)$ and $\sigma = 0.075$. This boundary profile perturbs
 319 the unit disk inwards near $\theta = \pi$ and outwards near $\theta = 0$. For $m = 3$, in Fig. 5 we
 320 show a favorable comparison between the full numerical PDE results and the hybrid
 321 results for the optimal average MFPT and trap locations. Moreover, from the two
 322 rightmost plots in Fig. 4, we observe that there are two five-trap patterns that give
 323 local minima for \bar{u}_0 . The pattern that has a trap on the line of symmetry near the

324 outward bulge at $\theta = 0$ is, in this case, not a global minimum of the average MFPT.
 325 This indicates that hard-to-assess global effects, rather than simply the local geometry
 326 near a protrusion, play a central role for characterizing the optimal trap pattern.

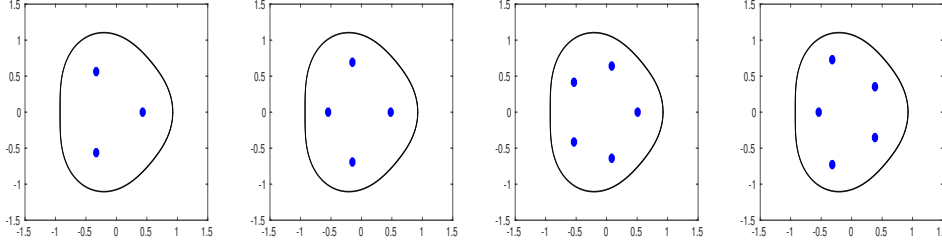


FIG. 4. *Optimal trap patterns for $D = 1$ in a near-disk domain with boundary $r = 1 + \sigma h(\theta)$, $\sigma = 0.075$ and $h(\theta) = \cos(3\theta) - \cos(\theta) - \cos(2\theta)$, that contains m traps of a common radius $\varepsilon = 0.05$. Computed from minimizing (2.26) using the ODE relaxation scheme (3.4). Left: $m = 3$ and $\bar{u} \approx 0.2794$. Left-Middle: $m = 4$ and $\bar{u} \approx 0.19055$. Right-Middle: $m = 5$ and $\bar{u} \approx 0.1418$. Right: $m = 5$, $\bar{u} \approx 0.1383$. The two patterns for $m = 5$ are local minimizers, with rather close values for \bar{u} . The global minimum is achieved for the rightmost pattern.*

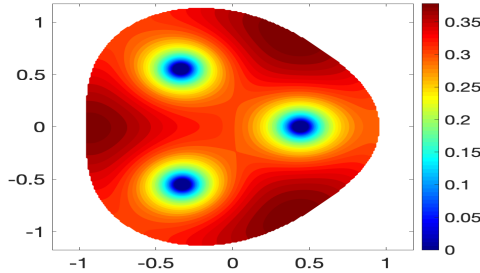


FIG. 5. *Contour plot of the PDE numerical solution for the optimal average MFPT and trap locations computed from the closest point method corresponding to the parameter values in the left panel of Fig. 4. Full PDE results for optimal locations: $(-0.3382, 0.5512)$, $(-0.3288, -0.5510)$, $(0.4410, 0.0012)$, and $\bar{u} = 0.2996$. Hybrid results: $(-0.3316, 0.5626)$, $(-0.3316, 0.5626)$, $(0.4314, 0.000)$, and $\bar{u}_0 = 0.2794$.*

327 **4. Optimizing Trap Configurations for the MFPT in an Ellipse.** Next,
 328 we consider the trap optimization problem in an ellipse of arbitrary aspect ratio, but
 329 with fixed area π . Our analysis uses a new explicit analytical formula, as derived in
 330 § 5, for the Neumann Green's function $G(\mathbf{x}; \mathbf{x}_0)$ and its regular part R_e of (5.1).

331 For m circular traps each of radius ε , the average MFPT \bar{u}_0 satisfies (see (2.16))

$$332 \quad (4.1) \quad \bar{u}_0 = \frac{|\Omega|}{2\pi D\nu m} + \frac{2\pi}{m} \mathbf{e}^T \mathcal{G} \mathcal{A}, \quad \text{where} \quad \left[I + 2\pi\nu(I - E)\mathcal{G} \right] \mathcal{A} = \frac{|\Omega|}{2\pi Dm} \mathbf{e}.$$

333 Here $E \equiv \mathbf{e}\mathbf{e}^T/m$, $\mathbf{e} = (1, \dots, 1)^T$, $\nu \equiv -1/\log \varepsilon$, and the Green's matrix \mathcal{G} depends
 334 on the trap locations $\{\mathbf{x}_1, \dots, \mathbf{x}_m\}$. To determine optimal trap configurations that are
 335 minimizers of the average MFPT, given in (4.1), we use the ODE relaxation scheme

$$336 \quad (4.2) \quad \frac{d\mathbf{z}}{dt} = -\nabla_{\mathbf{z}} \bar{u}_0, \quad \text{where} \quad \mathbf{z} \equiv (x_1, y_1, \dots, x_m, y_m).$$

337 In our implementation of (4.2), the gradient was approximated using a centered dif-
 338 ference scheme with mesh spacing 10^{-4} . The results shown below for the optimal trap
 339 patterns are confirmed from using a particle swarm approach [11].

340 The derivation of the Neumann Green's function and its regular part in § 5 is
 341 based on mapping the elliptical domain to a rectangular domain using

$$342 \quad (4.3a) \quad x = f \cosh \xi \cos \eta, \quad y = f \sinh \xi \sin \eta, \quad f = \sqrt{a^2 - b^2}.$$

343 With these elliptic cylindrical coordinates, the ellipse is mapped to the rectangle
 344 $0 \leq \xi \leq \xi_b$ and $0 \leq \eta \leq 2\pi$, where $a = f \cosh \xi_b$ and $b = f \sinh \xi_b$, so that

$$345 \quad (4.3b) \quad f = \sqrt{a^2 - b^2}, \quad \xi_b = \tanh^{-1} \left(\frac{b}{a} \right) = -\frac{1}{2} \log \beta, \quad \beta \equiv \left(\frac{a-b}{a+b} \right).$$

346 To determine (ξ, η) , given a pair (x, y) , we invert the transformation (4.3a) using
 (4.4a)

$$347 \quad \xi = \frac{1}{2} \log \left(1 - 2s + 2\sqrt{s^2 - s} \right), \quad s \equiv \frac{-\mu - \sqrt{\mu^2 + 4f^2 y^2}}{2f^2}, \quad \mu \equiv x^2 + y^2 - f^2.$$

348 To recover η , we define $\eta_* \equiv \sin^{-1}(\sqrt{p})$ and use

$$349 \quad (4.4b) \quad \eta = \begin{cases} \eta_*, & \text{if } x \geq 0, y \geq 0 \\ \pi - \eta_*, & \text{if } x < 0, y \geq 0 \\ \pi + \eta_*, & \text{if } x \leq 0, y < 0 \\ 2\pi - \eta_*, & \text{if } x > 0, y < 0 \end{cases}, \quad \text{where } p \equiv \frac{-\mu + \sqrt{\mu^2 + 4f^2 y^2}}{2f^2}.$$

350 As derived in § 5, the matrix entries in \mathcal{G} are obtained from the explicit result

$$351 \quad (4.5a) \quad G(\mathbf{x}; \mathbf{x}_0) = \frac{1}{4|\Omega|} (|\mathbf{x}|^2 + |\mathbf{x}_0|^2) - \frac{3}{16|\Omega|} (a^2 + b^2) - \frac{1}{4\pi} \log \beta - \frac{1}{2\pi} \xi_{>} \\ - \frac{1}{2\pi} \sum_{n=0}^{\infty} \log \left(\prod_{j=1}^8 |1 - \beta^{2n} z_j| \right), \quad \text{for } \mathbf{x} \neq \mathbf{x}_0,$$

352 where $|\Omega| = \pi ab$, $\xi_{>} \equiv \max(\xi, \xi_0)$, and the complex constants z_1, \dots, z_8 are defined
 353 in terms of (ξ, η) , (ξ_0, η_0) and ξ_b by

$$(4.5b) \\ 354 \quad \begin{aligned} z_1 &\equiv e^{-|\xi - \xi_0| + i(\eta - \eta_0)}, & z_2 &\equiv e^{|\xi - \xi_0| - 4\xi_b + i(\eta - \eta_0)}, & z_3 &\equiv e^{-(\xi + \xi_0) - 2\xi_b + i(\eta - \eta_0)}, \\ z_4 &\equiv e^{\xi + \xi_0 - 2\xi_b + i(\eta - \eta_0)}, & z_5 &\equiv e^{\xi + \xi_0 - 4\xi_b + i(\eta + \eta_0)}, & z_6 &\equiv e^{-(\xi + \xi_0) + i(\eta + \eta_0)}, \\ z_7 &\equiv e^{|\xi - \xi_0| - 2\xi_b + i(\eta + \eta_0)}, & z_8 &\equiv e^{-|\xi - \xi_0| - 2\xi_b + i(\eta + \eta_0)}. \end{aligned}$$

355 Observe that the Dirac point at $\mathbf{x}_0 = (x_0, y_0)$ is mapped to (ξ_0, η_0) . The transforma-
 356 tion (4.3) and its inverse (4.4), determines $G(\mathbf{x}; \mathbf{x}_0)$ explicitly in terms of $\mathbf{x} \in \Omega$.

357 Moreover, as shown in § 5, the regular part of the Neumann Green's function, R_e ,
 358 satisfying $G(\mathbf{x}; \mathbf{x}_0) \sim -(2\pi)^{-1} \log |\mathbf{x} - \mathbf{x}_0| + R_e$ as $\mathbf{x} \rightarrow \mathbf{x}_0$, is given by

$$(4.6a) \\ 359 \quad R_e = \frac{|\mathbf{x}_0|^2}{2|\Omega|} - \frac{3}{16|\Omega|} (a^2 + b^2) + \frac{1}{2\pi} \log(a+b) - \frac{\xi_0}{2\pi} + \frac{1}{4\pi} \log(\cosh^2 \xi_0 - \cos^2 \eta_0) \\ - \frac{1}{2\pi} \sum_{n=1}^{\infty} \log(1 - \beta^{2n}) - \frac{1}{2\pi} \sum_{n=0}^{\infty} \log \left(\prod_{j=2}^8 |1 - \beta^{2n} z_j^0| \right).$$

360 Here, z_j^0 is the limiting value of z_j , defined in (4.5b), as $(\xi, \eta) \rightarrow (\xi_0, \eta_0)$, given by

$$361 \quad (4.6b) \quad \begin{aligned} z_2^0 &= \beta^2, & z_3^0 &= \beta e^{-2\xi_0}, & z_4^0 &= \beta e^{2\xi_0}, & z_5^0 &= \beta^2 e^{2\xi_0 + 2i\eta_0}, \\ z_6^0 &= e^{-2\xi_0 + 2i\eta_0}, & z_7^0 &= \beta e^{2i\eta_0}, & z_8^0 &= \beta e^{2i\eta_0}, & \text{where } \beta &\equiv \frac{a-b}{a+b}. \end{aligned}$$

362 **4.1. Examples of the Theory.** In this subsection, we will apply our hybrid
 363 analytical-numerical approach based on (4.1), (4.5), (4.6) and the ODE relaxation
 364 scheme (4.2), to compute optimal trap configurations in an elliptical domain of area π
 365 with either $m = 2, \dots, 5$ circular traps of a common radius $\varepsilon = 0.05$. In our examples
 366 below, we set $D = 1$ and we study how the optimal pattern of traps changes as
 367 the aspect ratio of the ellipse is varied. We will compare our results from this hybrid
 368 theory with the near-disk asymptotic results of (2.26), with full PDE numerical results
 369 computed from the closest point method [10], and with the asymptotic approximations
 370 derived below in § 4.2, which are valid for a long and thin ellipse.

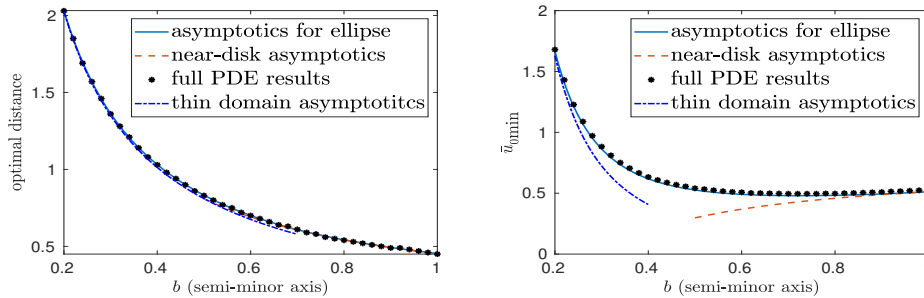


FIG. 6. The optimal trap distance from the origin (left panel) and optimal average MFPT \bar{u}_{0min} (right panel) versus the semi-minor axis b of an elliptical domain of area π that contains two traps of a common radius $\varepsilon = 0.05$ and $D = 1$. The optimum trap locations are on the semi-major axis, equidistant from the origin. Solid curves: hybrid asymptotic theory (4.1) for the ellipse coupled to the ODE relaxation scheme (4.2) to find the minimum. Dashed line (red): near-disk asymptotics of (2.26). Discrete points: full numerical PDE results computed from the closest point method. Dashed-dotted line (blue): thin-domain asymptotics (4.14). These curves essentially overlap with those from the hybrid theory for the optimal trap distance.

371 For $m = 2$ traps, in the right panel of Fig. 6 we show results for the optimal
 372 average MFPT versus the semi-minor axis b of the ellipse. The hybrid theory is
 373 seen to compare very favorably with full numerical PDE results for all $b \leq 1$. For
 374 b near unity and for b small, the near-disk theory of (2.26) and (3.4), and the thin-
 375 domain asymptotic result in (4.14) are seen to provide, respectively, good predictions
 376 for the optimal MFPT. Our hybrid theory shows that the optimal trap locations
 377 are on the semi-major axis for all $b < 1$. In the left panel of Fig. 6, the optimal
 378 trap locations found from the steady-state of our ODE relaxation (4.2) are seen to
 379 compare very favorably with full PDE results. Remarkably, we observe that the thin-
 380 domain asymptotics prediction in (4.14) agrees well with the optimal locations from
 381 our hybrid theory for $b < 0.7$.

382 Next, we consider the case $m = 3$. To clearly illustrate how the optimal trap
 383 configuration changes as the aspect ratio of the ellipse is varied, we use the hybrid
 384 theory to compute the area of the triangle formed by the three optimally located
 385 traps. The results shown in Fig. 7 are seen to compare favorably with full PDE
 386 results. These results show that the optimal traps become colinear on the semi-
 387 major axis when $a \geq 1.45$. In Fig. 8 we show snapshots, at certain values of the

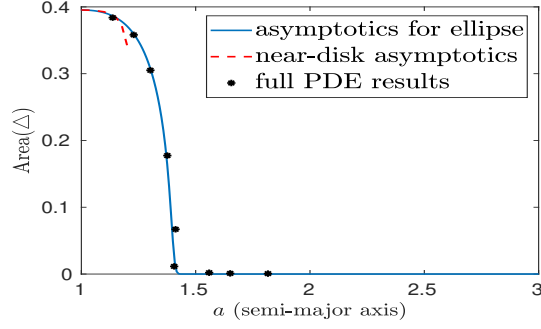


FIG. 7. Area of the triangle formed by the three optimally located traps of a common radius $\varepsilon = 0.05$ with $D = 1$ in a deforming ellipse of area π versus versus the semi-major axis a . The optimal traps become collinear as a increases. Solid curve: hybrid asymptotic theory (4.1) for the ellipse coupled to the ODE relaxation scheme (4.2) to find the minimum. Dashed line: near-disk asymptotics of (2.26). Discrete points: full numerical PDE results computed from the closest point method.

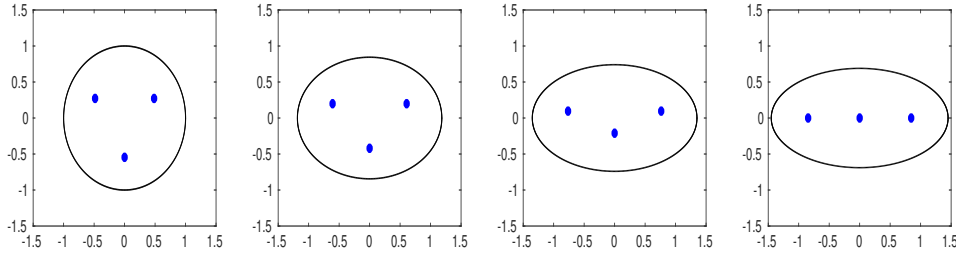


FIG. 8. Optimal three-trap configurations for $D = 1$ in a deforming ellipse of area π with semi-major axis a and a common trap radius $\varepsilon = 0.05$. Left: $a = 1$, $b = 1$. Middle Left: $a = 1.184$, $b \approx 0.845$. Middle Right: $a = 1.351$, $b \approx 0.740$. Right: $a = 1.450$, $b \approx 0.690$. The optimally located traps form an isosceles triangle as they deform from a ring pattern in the unit disk to a collinear pattern as a increases.

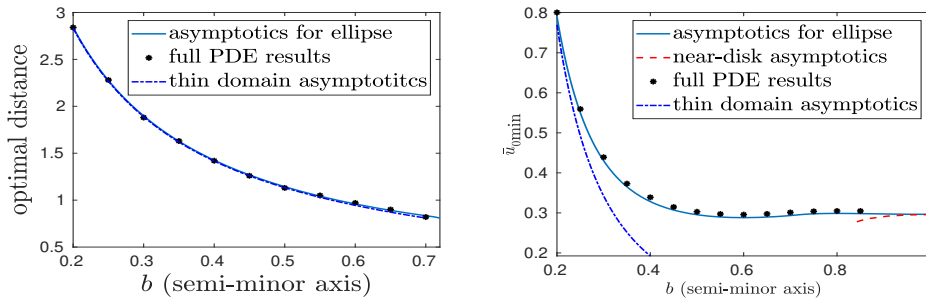


FIG. 9. Left panel: Optimal distance from the origin for a collinear three-trap pattern on the major-axis of an ellipse of area π versus the semi-minor axis b . When $b \leq 0.71$ the optimal pattern has a trap at the center and a pair of traps symmetrically located on either side of the origin. Right panel: optimal average MFPT \bar{u}_{\min} versus b . Solid curves: hybrid asymptotic theory (4.1) for the ellipse coupled to the ODE relaxation scheme (4.2) to find the minimum. Dashed line (red): near-disk asymptotics of (2.26). Discrete points: Full PDE numerical results computed using the closest point method. Dashed-dotted line (blue): thin-domain asymptotics (4.17).

388 semi-major axis, of the optimal trap locations in the ellipse. In the right panel of
 389 Fig. 9, we show that the optimal average MFPT from the hybrid theory compares
 390 very well with full numerical PDE results for all $b \leq 1$, and that the thin domain
 391 asymptotics (4.17) provides a good approximation when $b \leq 0.3$. In the left panel of
 392 Fig. 9 we plot the optimal trap locations on the semi-major axis when the trap pattern
 393 is collinear. We observe that results for the optimal trap locations from the hybrid
 394 theory, the thin domain asymptotics (4.17), and the full PDE simulations, essentially
 395 coincide on the full range $0.2 < b < 0.7$.

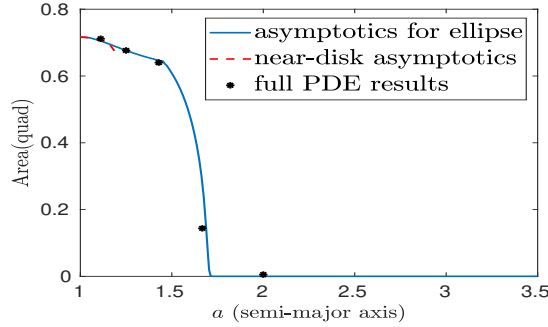


FIG. 10. Area of the quadrilateral formed by the four optimally located traps of a common radius $\varepsilon = 0.05$ with $D = 1$ in a deforming ellipse of area π and semi-major axis a . The optimal traps become collinear as a increases. Solid curve: hybrid asymptotic theory (4.1) for the ellipse coupled to the ODE relaxation scheme (4.2) to find the minimum. Dashed line (red): near-disk asymptotics of (2.26). Discrete points: full numerical PDE results computed from the closest point method.

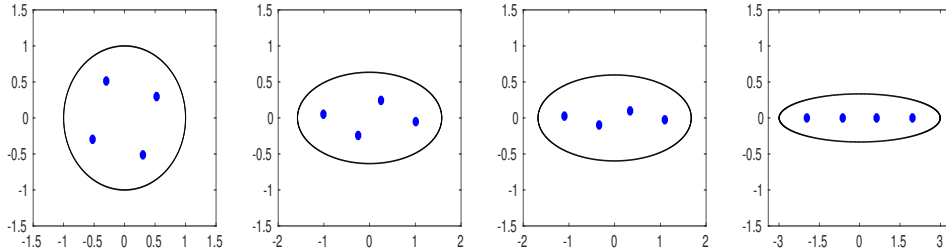


FIG. 11. Optimal four-trap configurations for $D = 1$ in a deforming ellipse of area π with semi-major axis a and a common trap radius $\varepsilon = 0.05$. Left: $a = 1$, $b = 1$. Middle Left: $a = 1.577$, $b \approx 0.634$. Middle Right: $a = 1.675$, $b \approx 0.597$. Right: $a = 3.0$, $b \approx 0.333$. The optimally located traps form a rectangle, followed by a parallelogram, as they deform from a ring pattern in the unit disk to a collinear pattern as a increases.

396 For the case of four traps, where $m = 4$, in Fig. 10 we use the hybrid theory to
 397 plot the area of the quadrilateral formed by the four optimally located traps versus
 398 the semi-major axis $a > 1$. The full PDE results, also shown in Fig. 10, compare
 399 well with the hybrid results. This figure shows that as the aspect ratio of the ellipse
 400 increases the traps eventually become collinear on the semi-major axis when $a \geq 1.7$.
 401 This feature is further illustrated by the snapshots of the optimal trap locations shown
 402 in Fig. 11 at representative values of a . In the right panel of Fig. 12, we show that
 403 the hybrid and full numerical PDE results for the optimal average MFPT agree very
 404 closely for all $b \leq 1$, but that the thin-domain asymptotic result (4.20) agrees well only

405 when $b \leq 0.25$. However, as similar to the three-trap case, on the range of b where the
 406 trap pattern is collinear, in the left panel of Fig. 12 we show that the hybrid theory,
 407 the full PDE simulations, and the thin-domain asymptotics all provide essentially
 408 indistinguishable predictions for the optimal trap locations on the semi-major axis.

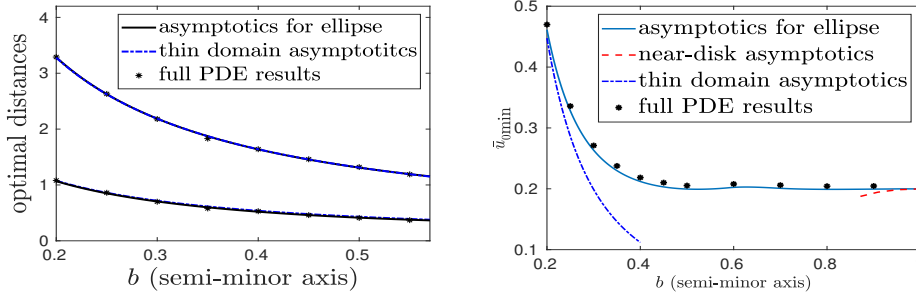


FIG. 12. *Left panel: Optimal distances from the origin for a collinear four-trap pattern on the major-axis of an ellipse of area π and semi-minor axis b . When $b \leq 0.57$ the optimal pattern has two pairs of traps symmetrically located on either side of the origin. Right panel: the optimal average MFPT \bar{u}_{omin} versus b . Solid curves: hybrid asymptotic theory (4.1) for the ellipse coupled to the ODE relaxation scheme (4.2) to find the minimum. Dashed line (red): near-disk asymptotics of (2.26). Discrete points: full numerical PDE results computed from the closest point method. Dashed-dotted line (blue): thin-domain asymptotics (4.20).*

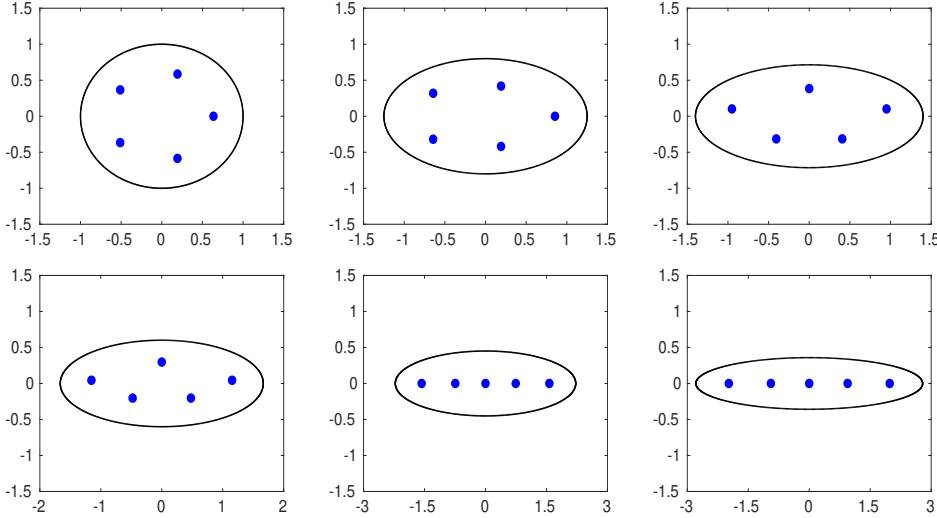


FIG. 13. *Optimal five-trap configurations for $D = 1$ in a deforming ellipse of area π with semi-major axis a and a common trap radius $\varepsilon = 0.05$. Top left: $a = 1, b = 1$. Top middle: $a = 1.25, b = 0.8$. Top right: $a = 1.4, b \approx 0.690$. Bottom left: $a = 1.665, b \approx 0.601$. Bottom middle: $a = 2.22, b \approx 0.450$. Bottom right: $a = 2.79, b \approx 0.358$. The optimal traps become collinear as a increases and the edge-most traps become closer to the corner of the domain as a increases.*

409 Finally, we show similar results for the case of five traps. In Fig. 13, we plot the
 410 optimal trap locations in the ellipse as the semi-major axis of the ellipse is varied.
 411 This plot shows that the optimal pattern becomes collinear when (roughly) $a \geq 2$.
 412 In the right panel of Fig. 14, we show a close agreement between the hybrid and full

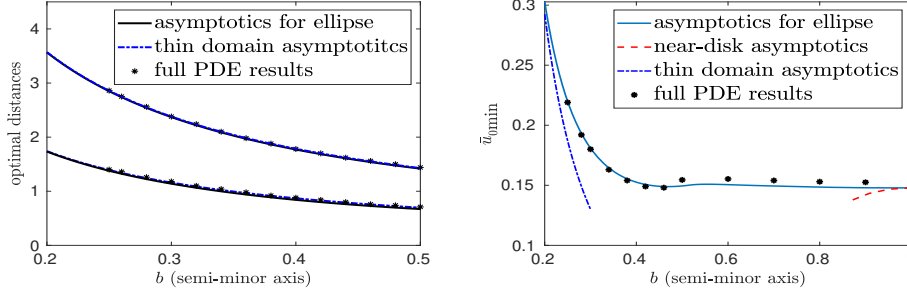


FIG. 14. *Left panel: Optimal distances from the origin for a collinear five-trap pattern on the major-axis of an ellipse of area π and semi-minor axis b . When $b \leq 0.51$ the optimal pattern has a trap at the center and two pairs of traps symmetrically located on either side of the origin. Right panel: The optimal average MFPT \bar{u}_{0min} versus b . Solid curves: hybrid asymptotic theory for the ellipse (4.1) coupled to the ODE relaxation scheme (4.2) to find the minimum. Dashed line (red): near-disk asymptotics of (2.26). Discrete points: full numerical PDE results computed from the closest point method. Dashed-dotted line (blue): thin-domain asymptotics (4.22).*

numerical PDE results for the optimal average MFPT. However, as seen in Fig. 14, the thin-domain asymptotic result (4.22) accurately predicts the optimal MFPT only for rather small b . As for the four-trap case, in the left panel of Fig. 14 we show that the hybrid theory, the full PDE simulations, and the thin-domain asymptotics all yield similar predictions for the optimal trap locations on the semi-major axis.

4.2. Thin-Domain Asymptotics. For a long and thin ellipse, where $b = \delta \ll 1$ and $a = 1/\delta$ but with $|\Omega| = \pi$, we now derive simple approximations for the optimal trap locations and the optimal average MFPT using an approach based on thin-domain asymptotics. For $m = 2$ the optimal trap locations are on the semi-major axis (cf. Fig. 6), while for $3 \leq m \leq 5$ the optimal trap locations become collinear when the semi-minor axis b decreases below a threshold (see Fig. 8, Fig. 11, and Fig. 13).

As derived in Appendix A, the leading-order approximation for the MFPT u satisfying (2.2) in a thin elliptical with $b = \delta \ll 1$ is

$$(4.7) \quad u(x, y) \sim \delta^{-2} U_0(\delta x) + \mathcal{O}(\delta^{-1}),$$

where the one-dimensional profile $U_0(X)$, with $x = X/\delta$, satisfies the ODE

$$(4.8) \quad \left[\sqrt{1 - X^2} U_0' \right]' = -\frac{\sqrt{1 - X^2}}{D}, \quad \text{on } |X| \leq 1,$$

with U_0 and U_0' bounded as $X \rightarrow \pm 1$. In terms of $U_0(X)$, the average MFPT for the thin ellipse is estimated for $\delta \ll 1$ as

$$(4.9) \quad \bar{u}_0 \sim \frac{1}{\pi} \int_{-1/\delta}^{1/\delta} \int_{-\delta\sqrt{1-\delta^2 x^2}}^{\delta\sqrt{1-\delta^2 x^2}} u \, dx dy \sim \frac{4}{\pi\delta^2} \int_0^1 \sqrt{1 - X^2} U_0(X) \, dX.$$

In the thin domain limit, the circular traps of a common radius ε centered on the semi-major axis are approximated by zero point constraints for U_0 at locations on the interval $|X| \leq 1$. In this way, (4.8) becomes a multi-point BVP problem, whose solution depends on the locations of the zero point constraints. Optimal values for the location of these constraints are obtained by minimizing the 1-D integral in (4.9) approximating \bar{u}_0 . We now apply this approach for $m = 2, \dots, 5$ collinear traps.

438 For $m = 2$ traps centered at $X = \pm d$ with $0 < d < 1$, the multi-point BVP for
 439 $U_0(X)$ on $0 < X < 1$ satisfies

$$440 \quad (4.10) \quad \left[\sqrt{1 - X^2} U_0' \right]' = -\frac{\sqrt{1 - X^2}}{D}, \quad 0 < X < 1; \quad U_0'(0) = 0, \quad U_0(d) = 0,$$

441 with U_0 and U_0' bounded as $X \rightarrow \pm 1$. A particular solution for (4.10) is $U_{0p} =$
 442 $-[(\sin^{-1}(X))^2 + X^2]/(4D)$, while the homogeneous solution is $U_{0H} = c_1 \sin^{-1}(X) +$
 443 c_2 . By combining these solutions, we readily calculate that

$$444 \quad (4.11a) \quad U_0(X) = \begin{cases} -\frac{1}{4D} \left[(\sin^{-1} X)^2 + X^2 - \pi \sin^{-1} X + c_2 \right], & d \leq X \leq 1, \\ -\frac{1}{4D} \left[(\sin^{-1} X)^2 + X^2 + c_1 \right], & 0 \leq X \leq d, \end{cases}$$

445 where c_1 and c_2 are given by

$$446 \quad (4.11b) \quad c_1 = -d^2 - (\sin^{-1} d)^2, \quad c_2 = -d^2 + \pi \sin^{-1} d - (\sin^{-1} d)^2.$$

447 Upon substituting (4.11a) into (4.9), we obtain that

$$448 \quad (4.12a) \quad \bar{u}_0 \sim -\frac{1}{\pi D \delta^2} [J_0 + \mathcal{H}(d)],$$

449 where the two integrals J_0 and $\mathcal{H}(d)$ are given by

$$450 \quad (4.12b) \quad J_0 \equiv \int_0^1 F(X) \left[(\sin^{-1} X)^2 + X^2 - \pi \sin^{-1}(X) \right] dX \approx -0.703,$$

$$451 \quad (4.12c) \quad \mathcal{H}(d) \equiv \pi \int_0^d F(X) \sin^{-1}(X) dX + c_2 \int_d^1 F(X) dX + c_1 \int_0^d F(X) dX,$$

453 where $F(X) = \sqrt{1 - X^2}$. By performing a few quadratures, and using (4.11b) for c_1
 454 and c_2 , we obtain an explicit expression for $\mathcal{H}(d)$:

$$455 \quad (4.13) \quad \mathcal{H}(d) = -\frac{\pi}{2} [\sin^{-1}(d)]^2 + \frac{\pi^2}{4} \sin^{-1}(d) - \frac{\pi d^2}{2}.$$

456 To estimate the optimal average MFPT we simply maximize $\mathcal{H}(d)$ in (4.13)
 457 on $0 < d < 1$. We compute that $d_{\text{opt}} \approx 0.406$, and correspondingly $\bar{u}_{0\text{min}} =$
 458 $-(\pi D \delta^2)^{-1} [J_0 + \mathcal{H}(d_{\text{opt}})]$. Then, by setting $\delta = b$ and $x_{\text{opt}} = d_{\text{opt}}/\delta$, we obtain
 459 the following estimate for the optimal trap location and minimum average MFPT for
 460 $m = 2$ traps in the thin domain limit:

$$461 \quad (4.14) \quad x_{0\text{opt}} \sim 0.406/b, \quad \bar{u}_{0\text{opt}} \sim 0.0652/(b^2 D), \quad \text{for } b \ll 1.$$

462 These estimates are favorably compared in Fig. 6 with full PDE solutions computed
 463 using the closest point method [10] and with the full asymptotic theory based on (4.1).

464 Next, suppose that $m = 3$. Since there is an additional trap at the origin, we
 465 simply replace the condition $U_0'(0) = 0$ in (4.10) with $U_0(0) = 0$. In place of (4.11a),

$$466 \quad (4.15a) \quad U_0(X) = \begin{cases} -\frac{1}{4D} \left[(\sin^{-1} X)^2 + X^2 - \pi \sin^{-1} X + c_2 \right], & d \leq X \leq 1, \\ -\frac{1}{4D} \left[(\sin^{-1} X)^2 + X^2 + c_1 \sin^{-1} X \right], & 0 \leq X \leq d, \end{cases}$$

467 where c_1 and c_2 are given by
 (4.15b)

$$468 \quad c_1 = -\left(d^2 + [\sin^{-1}(d)]^2\right) / \sin^{-1}(d), \quad c_2 = -d^2 + \pi \sin^{-1}(d) - [\sin^{-1}(d)]^2 .$$

469 The average MFPT is given by (4.12a), where $\mathcal{H}(d)$ is now defined by

$$470 \quad (4.16) \quad \mathcal{H}(d) \equiv c_2 \int_d^1 F(X) dX + (c_1 + \pi) \int_0^d F(X) \sin^{-1}(X) dX ,$$

471 with $F(X) = \sqrt{1 - X^2}$. By maximizing $\mathcal{H}(d)$ on $0 < d < 1$, we obtain $d_{\text{opt}} \approx 0.567$,
 472 so that $\bar{u}_{\text{0min}} = -(\pi D \delta^2)^{-1} [J_0 + \mathcal{H}(d_{\text{opt}})]$. In this way, the optimal trap location
 473 and the minimum of the average MFPT satisfies

$$474 \quad (4.17) \quad x_{0\text{opt}} \sim 0.567/b, \quad \bar{u}_{0\text{opt}} \sim 0.0308/(b^2 D), \quad \text{for } b \ll 1 .$$

475 In Fig. 9 these scaling laws are seen to compare well with full PDE solutions and with
 476 the full asymptotic theory of (4.1), even when b is only moderately small.

477 Next, we consider the case $m = 4$, with two symmetrically placed traps on either
 478 side of the origin. Therefore, we solve (4.10) with $U'_0(0) = 0$, $U_0(d_1) = 0$, and
 479 $U_0(d_2) = 0$, where $0 < d_1 < d_2$. In place of (4.11a), we get

$$480 \quad (4.18a) \quad U_0(X) = \begin{cases} -\frac{1}{4D} \left[(\sin^{-1} X)^2 + X^2 - \pi \sin^{-1} X + c_2 \right], & d_2 \leq X \leq 1, \\ -\frac{1}{4D} \left[(\sin^{-1} X)^2 + X^2 + b_1 \sin^{-1} X + b_2 \right], & d_1 \leq X \leq d_2, \\ -\frac{1}{4D} \left[(\sin^{-1} X)^2 + X^2 + c_1 \right], & 0 \leq X \leq d_1, \end{cases}$$

481 where c_1 and c_2 are given by

(4.18b)

$$482 \quad c_1 = -d_1^2 - (\sin^{-1} d_1)^2, \quad c_2 = -d_2^2 + \pi \sin^{-1} d_2 - (\sin^{-1} d_2)^2, \\ b_1 = \frac{(\sin^{-1} d_1)^2 - (\sin^{-1} d_2)^2 + d_1^2 - d_2^2}{\sin^{-1} d_2 - \sin^{-1} d_1}, \quad b_2 = -b_1 \sin^{-1} d_1 - d_1^2 - (\sin^{-1} d_1)^2 .$$

483 The average MFPT is given by (4.12a), where $\mathcal{H} = \mathcal{H}(d_1, d_2)$ is now given by

(4.19)

$$484 \quad \mathcal{H}(d_1, d_2) \equiv c_2 \int_{d_2}^1 F(X) dX + (b_1 + \pi) \int_{d_1}^{d_2} F(X) \sin^{-1}(X) dX + b_2 \int_{d_1}^{d_2} F(X) dX \\ + \pi \int_0^{d_1} F(X) \sin^{-1}(X) dX + c_1 \int_0^{d_1} F(X) dX ,$$

485 where $F(X) \equiv \sqrt{1 - X^2}$. By using a grid search to maximize $\mathcal{H}(d_1, d_2)$ on $0 <$
 486 $d_1 < d_2 < 1$, we obtain that $d_{1\text{opt}} \approx 0.215$ and $d_{2\text{opt}} \approx 0.656$. This yields that the
 487 optimal trap locations and the minimum of the average MFPT, given by $\bar{u}_{\text{0min}} =$
 488 $-(\pi D \delta^2)^{-1} [J_0 + \mathcal{H}(d_{1\text{opt}}, d_{2\text{opt}})]$, have the scaling law

$$489 \quad (4.20) \quad x_{1\text{opt}} \sim 0.215/b, \quad x_{2\text{opt}} \sim 0.656/b, \quad \bar{u}_{0\text{opt}} \sim 0.0179/(b^2 D), \quad \text{for } b \ll 1 .$$

490 These scaling laws are shown in Fig. 12 to agree well with the full PDE solutions and
 491 with the full asymptotic theory of (4.1) when b is small.

492 Finally, we consider the case $m = 5$, where we need only modify the $m = 4$ analysis
 493 by adding a trap at the origin. Setting $U_0(0) = 0$, $U_0(d_1) = 0$, and $U_0(d_2) = 0$ we
 494 obtain that U_0 is again given by (4.18a), except that now c_1 in (4.18a) is replaced
 495 by $c_1 \sin^{-1}(X)$, with c_1 as defined in (4.15b). The average MFPT satisfies (4.12a),
 496 where in place of (4.19) we obtain that $\mathcal{H}(d_1, d_2)$ is given by

$$497 \quad (4.21) \quad \mathcal{H}(d_1, d_2) \equiv c_2 \int_{d_1}^1 F(X) dX + (b_1 + \pi) \int_{d_1}^{d_2} F(X) \sin^{-1}(X) dX \\ + b_2 \int_{d_1}^{d_2} F(X) dX + (c_1 + \pi) \int_0^{d_1} F(X) \sin^{-1} X dX,$$

498 with $F(X) = \sqrt{1 - X^2}$. A grid search yields that $\mathcal{H}(d_1, d_2)$ is maximized on $0 < d_1 <$
 499 $d_2 < 1$ when $d_{1\text{opt}} \approx 0.348$ and $d_{2\text{opt}} \approx 0.714$. In this way, the corresponding optimal
 500 trap locations and minimum average MFPT have the scaling law

$$501 \quad (4.22) \quad x_{1\text{opt}} \sim 0.348/b, \quad x_{2\text{opt}} \sim 0.714/b, \quad \bar{u}_{0\text{opt}} \sim 0.0117/(b^2 D), \quad \text{for } b \ll 1.$$

502 Fig. 14 shows that (4.22) compares well with the full PDE solutions and with the full
 503 asymptotic theory of (4.1) when b is small.

504 **5. An Explicit Neumann Green's Function for the Ellipse.** We derive the
 505 *new explicit formula* (4.5) for the Neumann Green's function and its regular part in
 506 (4.6) in terms of rapidly converging infinite series. This Green's function $G(\mathbf{x}; \mathbf{x}_0)$ for
 507 the ellipse $\Omega \equiv \{\mathbf{x} = (x, y) \mid x^2/a^2 + y^2/b^2 \leq 1\}$ is the unique solution to

$$508 \quad (5.1a) \quad \Delta G = \frac{1}{|\Omega|} - \delta(\mathbf{x} - \mathbf{x}_0) \quad \mathbf{x} \in \Omega; \quad \partial_n G = 0, \quad \mathbf{x} \in \partial\Omega;$$

$$509 \quad (5.1b) \quad G \sim -\frac{1}{2\pi} \log|\mathbf{x} - \mathbf{x}_0| + R_e + o(1) \quad \text{as } \mathbf{x} \rightarrow \mathbf{x}_0; \quad \int_{\Omega} G d\mathbf{x} = 0,$$

511 where $|\Omega| = \pi ab$ is the area of Ω and R_e is the regular part of the Green's function.
 512 Here $\partial_n G$ is the outward normal derivative to the boundary of the ellipse. To remove
 513 the $|\Omega|^{-1}$ term in (5.1a), we introduce $N(\mathbf{x}; \mathbf{x}_0)$ defined by

$$514 \quad (5.2) \quad G(\mathbf{x}; \mathbf{x}_0) = \frac{1}{4|\Omega|} (x^2 + y^2) + N(\mathbf{x}; \mathbf{x}_0).$$

515 We readily derive that $N(\mathbf{x}; \mathbf{x}_0)$ satisfies

$$516 \quad (5.3a) \quad \Delta N = -\delta(\mathbf{x} - \mathbf{x}_0) \quad \mathbf{x} \in \Omega; \quad \partial_n N = -\frac{1}{2|\Omega|\sqrt{x^2/a^4 + y^2/b^4}}, \quad \mathbf{x} \in \partial\Omega;$$

$$517 \quad (5.3b) \quad \int_{\Omega} N d\mathbf{x} = -\frac{1}{4|\Omega|} \int_{\Omega} (x^2 + y^2) d\mathbf{x} = -\frac{1}{4|\Omega|} \left(\frac{|\Omega|}{4} (a^2 + b^2) \right) = -\frac{1}{16} (a^2 + b^2).$$

519 We assume that $a > b$, so that the semi-major axis is on the x -axis. To solve
 520 (5.3) we introduce the elliptic cylindrical coordinates (ξ, η) defined by (4.3) and its
 521 inverse mapping (4.4). We set $\mathcal{N}(\xi, \eta) \equiv N(x(\xi, \eta), y(\xi, \eta))$ and seek to convert (5.3)
 522 to a problem for \mathcal{N} defined in a rectangular domain. It is well-known that

$$523 \quad (5.4) \quad N_{xx} + N_{yy} = \frac{1}{f^2(\cosh^2 \xi - \cos^2 \eta)} (\mathcal{N}_{\xi\xi} + \mathcal{N}_{\eta\eta}).$$

524 Moreover, by computing the scale factors $h_\xi = \sqrt{x_\xi^2 + y_\xi^2}$ and $h_\eta = \sqrt{x_\eta^2 + y_\eta^2}$ of the
 525 transformation, we obtain that
 (5.5)

$$526 \quad \delta(x - x_0)\delta(y - y_0) = \frac{1}{h_\eta h_\xi} \delta(\xi - \xi_0)\delta(\eta - \eta_0) = \frac{1}{f^2(\cosh^2 \xi - \cos^2 \eta)} \delta(\xi - \xi_0)\delta(\eta - \eta_0),$$

527 where we used $h_\xi = h_\eta = f\sqrt{\cosh^2 \xi_0 - \cos^2 \eta_0}$. By using (5.4) and (5.5), we obtain
 528 that the PDE in (5.3a) transforms to

$$529 \quad (5.6) \quad \mathcal{N}_{\xi\xi} + \mathcal{N}_{\eta\eta} = -\delta(\xi - \xi_0)\delta(\eta - \eta_0), \quad \text{in } 0 \leq \eta \leq 2\pi, 0 \leq \xi \leq u_b.$$

530 To determine how the normal derivative in (5.3a) transforms, we calculate

$$531 \quad (5.7) \quad \begin{pmatrix} N_x \\ N_y \end{pmatrix} = \frac{1}{x_\xi y_\eta - x_\eta y_\xi} \begin{pmatrix} y_\eta & -y_\xi \\ -x_\eta & x_\xi \end{pmatrix} \begin{pmatrix} \mathcal{N}_\xi \\ \mathcal{N}_\eta \end{pmatrix},$$

532 where from (4.3a) we calculate

$$533 \quad (5.8) \quad x_\xi = f \sinh \xi \cos \eta = y_\eta, \quad x_\eta = -f \cosh \xi \sin \eta = -y_\xi.$$

534 Now using $x = a \cos \eta$ and $y = b \sin \eta$ on $\partial\Omega$, we calculate on $\partial\Omega$ that
 (5.9)

$$535 \quad \partial_n N = \nabla N \cdot \frac{(x/a^2, y/b^2)}{\sqrt{x^2/a^4 + y^2/b^4}} = \frac{(\frac{1}{a} \cos \eta, \frac{1}{b} \sin \eta)}{\sqrt{x^2/a^4 + y^2/b^4} (x_\xi y_\eta - x_\eta y_\xi)} \begin{pmatrix} y_\eta & -y_\xi \\ -x_\eta & x_\xi \end{pmatrix} \begin{pmatrix} \mathcal{N}_\xi \\ \mathcal{N}_\eta \end{pmatrix}.$$

536 By using (5.8), we calculate on $\partial\Omega$ that $x_\xi y_\eta - x_\eta y_\xi = b^2 \cos^2 \eta + a^2 \sin^2 \eta$. With this
 537 expression, we obtain after some algebra that (5.9) becomes

$$538 \quad (5.10) \quad \partial_n N = \frac{1}{ab\sqrt{x^2/a^4 + y^2/b^4}} \mathcal{N}_u, \quad \text{on } \xi = \xi_b.$$

539 By combining (5.10) and (5.3a), we obtain $\mathcal{N}_\xi = -1/(2\pi)$ on $\xi = \xi_b$.

540 Next, we discuss the other boundary conditions in the transformed plane. We
 541 require that \mathcal{N} and \mathcal{N}_η are 2π periodic in η . The boundary condition imposed on
 542 $\eta = 0$, which corresponds to the line segment $y = 0$ and $|x| \leq f = \sqrt{a^2 - b^2}$ between
 543 the two foci, is chosen to ensure that N and the normal derivative N_y are continuous
 544 across this segment. Recall from (4.4b) that the top of this segment $y = 0^+$ and
 545 $|x| \leq f$ corresponds to $0 \leq \eta \leq \pi$, while the bottom of this segment $y = 0^-$ and
 546 $|x| \leq f$ corresponds to $\pi \leq \eta \leq 2\pi$. To ensure that N is continuous across this
 547 segment, we require that $\mathcal{N}(\xi, \eta)$ satisfies $\mathcal{N}(0, \eta) = \mathcal{N}(0, 2\pi - \eta)$ for any $0 \leq \eta \leq \pi$.
 548 Moreover, since $\mathcal{N}_\xi = N_y f \sin \eta$ on $\xi = 0$, and $\sin(2\pi - \eta) = -\sin(\eta)$, we must have
 549 $\mathcal{N}_\xi(0, \eta) = \mathcal{N}_\xi(0, 2\pi - \eta)$ on $0 \leq \eta \leq \pi$.

550 Finally, we examine the normalization condition in (5.3b) by using

$$551 \quad (5.11) \quad \int_\Omega N(x, y) dx dy = \int_0^{\xi_b} \int_0^{2\pi} \mathcal{N}(\xi, \eta) \left| \det \begin{pmatrix} x_\xi & x_\eta \\ y_\xi & y_\eta \end{pmatrix} \right| d\xi d\eta.$$

552 Since $x_\xi y_\eta - x_\eta y_\xi = f^2 (\cosh^2 \xi - \cos^2 \eta)$, we obtain from (5.11) that (5.3b) becomes
 (5.12)

$$553 \quad \int_0^{\xi_b} \int_0^{2\pi} \mathcal{N}(\xi, \eta) [\cosh^2 \xi - \cos^2 \eta] d\xi d\eta = -\frac{1}{16f^2} (a^2 + b^2) = -\frac{(a^2 + b^2)}{16(a^2 - b^2)}.$$

554 In summary, from (5.6), (5.12), and the condition on $\xi = \xi_b$, $\mathcal{N}(\xi, \eta)$ satisfies

$$555 \quad (5.13a) \quad \Delta \mathcal{N} = -\delta(\xi - \xi_0)\delta(\eta - \eta_0) \quad 0 \leq \xi \leq \xi_b, \quad 0 \leq \eta \leq \pi,$$

$$556 \quad (5.13b) \quad \partial_\xi \mathcal{N} = -\frac{1}{2\pi}, \quad \text{on } \xi = \xi_b; \quad \mathcal{N}, \mathcal{N}_\eta \quad 2\pi \text{ periodic in } \eta,$$

$$557 \quad (5.13c) \quad \mathcal{N}(0, \eta) = \mathcal{N}(0, 2\pi - \eta), \quad \mathcal{N}_\xi(0, \eta) = -\mathcal{N}_\xi(0, 2\pi - \eta), \quad \text{for } 0 \leq \eta \leq \pi,$$

$$558 \quad (5.13d) \quad \int_0^{\xi_b} \int_0^{2\pi} \mathcal{N}(\xi, \eta) [\cosh^2 \xi - \cos^2 \eta] d\xi d\eta = -\frac{(a^2 + b^2)}{16(a^2 - b^2)}.$$

560 The solution to (5.13) is expanded in terms of the eigenfunctions in the η direction:

$$561 \quad (5.14) \quad \mathcal{N}(\xi, \eta) = \mathcal{A}_0(\xi) + \sum_{k=1}^{\infty} \mathcal{A}_k(\xi) \cos(k\eta) + \sum_{k=1}^{\infty} \mathcal{B}_k(\xi) \sin(k\eta).$$

562 The boundary condition (5.13b) is satisfied with $\mathcal{A}'_0(\xi_b) = -1/(2\pi)$ and $\mathcal{A}'_k(\xi_b) =$
 563 $\mathcal{B}'_k(\xi_b) = 0$, for $k \geq 1$. To satisfy $\mathcal{N}(0, \eta) = \mathcal{N}(0, 2\pi - \eta)$, we require $\mathcal{B}_k(0) = 0$ for
 564 $k \geq 1$. Finally, to satisfy $\mathcal{N}_\xi(0, \eta) = -\mathcal{N}_\xi(0, 2\pi - \eta)$, we require that $\mathcal{A}'_0(0) = 0$ and
 565 $\mathcal{A}'_k(0) = 0$ for $k \geq 1$. In the usual way, we can derive ODE boundary value problems
 566 for \mathcal{A}_0 , \mathcal{A}_k , and \mathcal{B}_k . We obtain that

$$567 \quad (5.15a) \quad \mathcal{A}_0'' = -\frac{1}{2\pi}\delta(\xi - \xi_0), \quad 0 \leq \xi \leq \xi_b; \quad \mathcal{A}'_0(0) = 0, \quad \mathcal{A}'_0(\xi_b) = -\frac{1}{2\pi},$$

568 while on $0 \leq \xi \leq \xi_b$, and for each $k = 1, 2, \dots$, we have

$$569 \quad (5.15b) \quad \mathcal{A}_k'' - k^2 \mathcal{A}_k = -\frac{1}{\pi} \cos(k\eta_0)\delta(\xi - \xi_0); \quad \mathcal{A}'_k(0) = 0, \quad \mathcal{A}'_k(\xi_b) = 0,$$

$$570 \quad (5.15c) \quad \mathcal{B}_k'' - k^2 \mathcal{B}_k = -\frac{1}{\pi} \sin(k\eta_0)\delta(\xi - \xi_0); \quad \mathcal{B}_k(0) = 0, \quad \mathcal{B}'_k(\xi_b) = 0.$$

572 We observe from (5.15a) that \mathcal{A}_0 is specified only up to an arbitrary constant.

573 We determine this constant from the normalization condition (5.13d). By substi-
 574 tuting (5.14) into (5.13d), we readily derive the identity that

$$575 \quad (5.16) \quad \int_0^{\xi_b} \mathcal{A}_0(\xi) \cosh(2\xi) d\xi - \frac{1}{2} \int_0^{\xi_b} \mathcal{A}_2(\xi) d\xi = -\frac{1}{16\pi} \left(\frac{a^2 + b^2}{a^2 - b^2} \right).$$

576 We will use (5.16) to derive a point constraint on $\mathcal{A}_0(\xi_b)$. To do so, we define $\phi(\xi) =$
 577 $\cosh(2\xi)$, which satisfies $\phi'' - 4\phi = 0$ and $\phi'(0) = 0$. We integrate by parts and use
 578 $\mathcal{A}'_0(0) = 0$ and $\mathcal{A}'_0(\xi_b) = -1/(2\pi)$ to get

$$579 \quad (5.17) \quad 4 \int_0^{\xi_b} \mathcal{A}_0 \phi d\xi = \int_0^{\xi_b} \mathcal{A}_0 \phi'' d\xi = (\phi' \mathcal{A}_0 - \phi \mathcal{A}'_0) \Big|_0^{\xi_b} + \int_0^{\xi_b} \phi \mathcal{A}_0'' d\xi,$$

$$= \phi'(\xi_b) \mathcal{A}_0(\xi_b) + \frac{1}{2\pi} [\phi(\xi_b) - \phi(\xi_0)].$$

580 Next, set $k = 2$ in (5.15b) and integrate over $0 < \xi < \xi_b$. Using the no-flux boundary
 581 conditions we get $\int_0^{\xi_b} \mathcal{A}_2 d\xi = \cos(2\eta_0)/(4\pi)$. We substitute this result, together with
 582 (5.17), into (5.16) and solve the resulting equation for $\mathcal{A}_0(\xi_b)$ to get

$$583 \quad (5.18) \quad \mathcal{A}_0(\xi_b) = \frac{1}{4\pi \sinh(2\xi_b)} \left[\cosh(2\xi_0) + \cos(2\eta_0) - \cosh(2\xi_b) - \frac{1}{2} \left(\frac{a^2 + b^2}{a^2 - b^2} \right) \right].$$

584 To simplify this expression we use $\tanh \xi_b = b/a$ to calculate $\sinh(2\xi_b) = 2ab/(a^2 - b^2)$
 585 and $\coth(2\xi_b) = (a^2 + b^2)/(2ab)$, while from (4.3a) we get

$$586 \quad x_0^2 + y_0^2 = f^2 [\cosh^2 \xi_0 - \sin^2 \eta_0] = \frac{(a^2 - b^2)}{2} [\cosh(2\xi_0) + \cos(2\eta_0)] .$$

587 Upon substituting these results into (5.18), we conclude that

$$588 \quad (5.19) \quad \mathcal{A}_0(\xi_b) = -\frac{3}{16|\Omega|}(a^2 + b^2) + \frac{1}{4|\Omega|}(x_0^2 + y_0^2) ,$$

589 where $|\Omega| = \pi ab$ is the area of the ellipse. With this explicit value for $\mathcal{A}_0(\xi_b)$, the nor-
 590 malization condition (5.13d), or equivalently the constraint $\int_{\Omega} G \, d\mathbf{x} = 0$, is satisfied.

591 Next, we solve the ODEs (5.15) for \mathcal{A}_0 , \mathcal{A}_k , and \mathcal{B}_k , for $k \geq 1$, to obtain

(5.20a)

$$592 \quad \mathcal{A}_0(\xi) = \frac{1}{2\pi} (\xi_b - \xi_>) + \mathcal{A}_0(\xi_b) , \quad \mathcal{A}_k(\xi) = \frac{\cos(k\eta_0)}{k\pi \sinh(k\xi_b)} \cosh(k\xi_<) \cosh(k(\xi_> - \xi_b)) ,$$

$$593 \quad (5.20b) \quad \mathcal{B}_k(\xi) = \frac{\sin(k\eta_0)}{k\pi \cosh(k\xi_b)} \sinh(k\xi_<) \cosh(k(\xi_> - \xi_b)) ,$$

594

595 where we have defined $\xi_> \equiv \max(\xi_0, \xi)$ and $\xi_< \equiv \min(\xi_0, \xi)$.

596 To determine an explicit expression for $G(\mathbf{x}; \mathbf{x}_0) = |\mathbf{x}|^2/(4|\Omega|) + \mathcal{N}(\xi, \eta)$, as given
 597 in (5.2), we substitute (5.19) and (5.20) into the eigenfunction expansion (5.14) for
 598 \mathcal{N} . In this way, we get

$$599 \quad (5.21a) \quad G(\mathbf{x}; \mathbf{x}_0) = \frac{1}{4|\Omega|} (|\mathbf{x}|^2 + |\mathbf{x}_0|^2) - \frac{3}{16|\Omega|}(a^2 + b^2) + \frac{1}{2\pi} (\xi_b - \xi_>) + \mathcal{S} ,$$

600 where the infinite sum \mathcal{S} is defined by

$$601 \quad (5.21b) \quad \mathcal{S} \equiv \sum_{k=1}^{\infty} \frac{\cos(k\eta_0) \cos(k\eta)}{\pi k \sinh(k\xi_b)} \cosh(k\xi_<) \cosh(k(\xi_> - \xi_b)) \\ + \sum_{k=1}^{\infty} \frac{\sin(k\eta_0) \sin(k\eta)}{\pi k \cosh(k\xi_b)} \sinh(k\xi_<) \cosh(k(\xi_> - \xi_b)) .$$

602 Next, from the product to sum formulas for $\cos(A) \cos(B)$ and $\sin(A) \sin(B)$ we get

$$603 \quad (5.22) \quad \mathcal{S} = \frac{1}{2\pi} \sum_{k=1}^{\infty} \frac{\cosh(k(\xi_> - \xi_b))}{k} \left[\frac{\cosh(k\xi_<)}{\sinh(k\xi_b)} + \frac{\sin(k\xi_<)}{\cosh(k\xi_b)} \right] \cos(k(\eta - \eta_0)) \\ + \frac{1}{2\pi} \sum_{k=1}^{\infty} \frac{\cosh(k(\xi_> - \xi_b))}{k} \left[\frac{\cosh(k\xi_<)}{\sinh(k\xi_b)} - \frac{\sin(k\xi_<)}{\cosh(k\xi_b)} \right] \cos(k(\eta + \eta_0)) .$$

604 Then, by using product to sum formulas for $\cosh(A) \cosh(B)$, the identity $\sinh(2A) =$
 605 $2 \sinh(A) \cosh(A)$, $\xi_> + \xi_< = \xi + \xi_0$, and $\xi_> - \xi_< = |\xi - \xi_0|$, some algebra yields that

$$606 \quad (5.23) \quad \mathcal{S} = \frac{1}{2\pi} \operatorname{Re} \left(\sum_{k=1}^{\infty} \frac{[\cosh(k(\xi + \xi_0)) + \cosh(k(|\xi - \xi_0| - 2\xi_b))]}{k \sinh(2k\xi_b)} e^{ik(\eta - \eta_0)} \right) \\ + \frac{1}{2\pi} \operatorname{Re} \left(\sum_{k=1}^{\infty} \frac{[\cosh(k(\xi + \xi_0 - 2\xi_b)) + \cosh(k|\xi - \xi_0|)]}{k \sinh(2k\xi_b)} e^{ik(\eta + \eta_0)} \right) .$$

607 The next step in the analysis is to convert the hyperbolic functions in (5.23) into
608 pure exponentials. A simple calculation yields that

$$609 \quad (5.24a) \quad \mathcal{S} = \frac{1}{2\pi} \operatorname{Re} \left(\sum_{k=1}^{\infty} \frac{\mathcal{H}_1}{k} e^{ik(\eta-\eta_0)} + \sum_{k=1}^{\infty} \frac{\mathcal{H}_2}{k} e^{ik(\eta+\eta_0)} \right),$$

610 where \mathcal{H}_1 and \mathcal{H}_2 are defined by

$$611 \quad (5.24b) \quad \mathcal{H}_1 \equiv \frac{1}{1 - e^{-4k\xi_b}} \left[e^{k(\xi+\xi_0-2\xi_b)} + e^{-k(\xi+\xi_0+2\xi_b)} + e^{k(|\xi-\xi_0|-4\xi_b)} + e^{-k|\xi-\xi_0|} \right],$$

$$\mathcal{H}_2 \equiv \frac{1}{1 - e^{-4k\xi_b}} \left[e^{k(\xi+\xi_0-4\xi_b)} + e^{k(|\xi-\xi_0|-2\xi_b)} + e^{-k(|\xi-\xi_0|+2\xi_b)} + e^{-k(\xi+\xi_0)} \right].$$

612 Then, for any q with $0 < q < 1$ and integer $k \geq 1$, we use the identity $\sum_{n=0}^{\infty} (q^k)^n =$
613 $\frac{1}{1-q^k}$ for the choice $q = e^{-4\xi_b}$, which converts \mathcal{H}_1 and \mathcal{H}_2 into infinite sums. This
614 leads to a doubly-infinite sum representation for \mathcal{S} in (5.24a) given by

$$615 \quad (5.25) \quad \mathcal{S} = \frac{1}{2\pi} \operatorname{Re} \left(\sum_{k=1}^{\infty} \sum_{n=0}^{\infty} \frac{(q^n)^k}{k} (z_1^k + z_2^k + z_3^k + z_4^k + z_5^k + z_6^k + z_7^k + z_8^k) \right),$$

616 where the complex constants z_1, \dots, z_8 are defined by (4.5b). From these formulae, we
617 readily observe that $|z_j| < 1$ on $0 \leq \xi \leq \xi_b$ for any $(\xi, \eta) \neq (\xi_0, \eta_0)$. Since $0 < q < 1$,
618 we can then switch the order of the sums in (5.25) when $(\xi, \eta) \neq (\xi_0, \eta_0)$ and use the
619 identity $\operatorname{Re} \left(\sum_{k=1}^{\infty} k^{-1} \omega^k \right) = -\log |1 - \omega|$, where $|1 - \omega|$ denotes modulus. In this
620 way, upon setting $\omega_j = q^n z_j$ for $j = 1, \dots, 8$, we obtain a compact representation for
621 \mathcal{S} . Finally, by using this result in (5.21) we obtain for $(\xi, \eta) \neq (\xi_0, \eta_0)$, or equivalently
622 $(x, y) \neq (x_0, y_0)$, the result given explicitly in (4.5) of § 4.

623 Next, to determine the regular part of the Neumann Green's function we must
624 identify the singular term in (4.5a) at $(\xi, \eta) = (\xi_0, \eta_0)$. Since $z_1 = 1$, while $|z_j| < 1$
625 for $j = 2, \dots, 8$, at $(\xi, \eta) = (\xi_0, \eta_0)$, the singular contribution arises only from the
626 $n = 0$ term in $\sum_{n=0}^{\infty} \log |1 - \beta^{2n} z_1|$. As such, we add and subtract the fundamental
627 singularity $-\log |\mathbf{x} - \mathbf{x}_0| / (2\pi)$ in (4.5a) to get

$$628 \quad (5.26a) \quad G(\mathbf{x}; \mathbf{x}_0) = -\frac{1}{2\pi} \log |\mathbf{x} - \mathbf{x}_0| + R(\mathbf{x}; \mathbf{x}_0),$$

629

$$630 \quad (5.26b) \quad R(\mathbf{x}; \mathbf{x}_0) = \frac{1}{4|\Omega|} (|\mathbf{x}|^2 + |\mathbf{x}_0|^2) - \frac{3(a^2 + b^2)}{16|\Omega|} - \frac{1}{4\pi} \log \beta - \frac{1}{2\pi} \xi_{\gt} + \frac{1}{2\pi} \log \left(\frac{|\mathbf{x} - \mathbf{x}_0|}{|1 - z_1|} \right)$$

$$- \frac{1}{2\pi} \sum_{n=1}^{\infty} \log |1 - \beta^{2n} z_1| - \frac{1}{2\pi} \sum_{n=0}^{\infty} \log \left(\prod_{j=2}^8 |1 - \beta^{2n} z_j| \right).$$

631 To identify $\lim_{\mathbf{x} \rightarrow \mathbf{x}_0} R(\mathbf{x}; \mathbf{x}_0) = R_e$, we must find $\lim_{\mathbf{x} \rightarrow \mathbf{x}_0} \log (|\mathbf{x} - \mathbf{x}_0| / |1 - z_1|)$.
632 To do so, we use a Taylor approximation on (4.3a) to derive at $(\xi, \eta) = (\xi_0, \eta_0)$ that

$$633 \quad (5.27) \quad \begin{pmatrix} \xi - \xi_0 \\ \eta - \eta_0 \end{pmatrix} = \frac{1}{(x_{\xi} y_{\eta} - x_{\eta} y_{\xi})} \begin{pmatrix} y_{\eta} & -x_{\eta} \\ -y_{\xi} & x_{\xi} \end{pmatrix} \begin{pmatrix} x - x_0 \\ y - y_0 \end{pmatrix}.$$

634 By calculating the partial derivatives in (5.27) using (5.8), and then noting from (4.5b)
635 that $|1 - z_1|^2 \sim (\xi - \xi_0)^2 + (\eta - \eta_0)^2$ as $(\xi, \eta) \rightarrow (\xi_0, \eta_0)$, we readily derive that

$$636 \quad (5.28) \quad \lim_{\mathbf{x} \rightarrow \mathbf{x}_0} \log \left(\frac{|\mathbf{x} - \mathbf{x}_0|}{|1 - z_1|} \right) = \frac{1}{2} \log (a^2 - b^2) + \frac{1}{2} \log (\cosh^2 \xi_0 - \cos^2 \eta_0).$$

637 Finally, we substitute (5.28) into (5.26b) and let $\mathbf{x} \rightarrow \mathbf{x}_0$. This yields the formula
 638 for the regular part of the Neumann Green's function as given in (4.6) of § 4. In
 639 Appendix B we show that the Neumann Green's function (4.5) for the ellipse reduces
 640 to the expression given in (3.1) for the unit disk when $a \rightarrow b = 1$.

641 **6. Discussion.** Here we discuss the relationship between our problem of optimal
 642 trap patterns and a related optimization problem for the fundamental Neumann ei-
 643 genvalue λ_0 of the Laplacian in a bounded 2-D domain Ω containing m small circular
 644 absorbing traps of a common radius ε . That is, λ_0 is the lowest eigenvalue of

$$645 \quad (6.1) \quad \begin{aligned} \Delta u + \lambda u &= 0, & x \in \Omega \setminus \cup_{j=1}^m \Omega_{\varepsilon j}; & \quad \partial_n u = 0, & x \in \partial\Omega, \\ u &= 0, & x \in \partial\Omega_{\varepsilon j}, & \quad j = 1, \dots, m. \end{aligned}$$

646 Here $\Omega_{\varepsilon j}$ is a circular disk of radius $\varepsilon \ll 1$ centered at $\mathbf{x}_j \in \Omega$. In the limit $\varepsilon \rightarrow$
 647 0, a two-term asymptotic expansion for λ_0 in powers of $\nu \equiv -1/\log \varepsilon$ is (see [12,
 648 Corollary 2.3] and Appendix C)

$$649 \quad (6.2) \quad \lambda_0 \sim \frac{2\pi m \nu}{|\Omega|} - \frac{4\pi^2 \nu^2}{|\Omega|} p(\mathbf{x}_1, \dots, \mathbf{x}_m) + \mathcal{O}(\nu^3), \quad \text{with } p(\mathbf{x}_1, \dots, \mathbf{x}_m) \equiv \mathbf{e}^T \mathcal{G} \mathbf{e},$$

650 where $\mathbf{e} \equiv (1, \dots, 1)^T$ and \mathcal{G} is the Neumann Green's matrix. To relate this result
 651 for λ_0 with that for the average MFPT \bar{u}_0 satisfying (4.1), we let $\nu \ll 1$ in (4.1) and
 652 calculate that $\mathcal{A} \sim |\Omega| \mathbf{e} / (2\pi D m) + \mathcal{O}(\nu)$. From (4.1), we conclude that

$$653 \quad (6.3) \quad \bar{u}_0 = \frac{|\Omega|}{2\pi D \nu m} \left(1 + \frac{2\pi \nu}{m} p(\mathbf{x}_1, \dots, \mathbf{x}_m) + \mathcal{O}(\nu^2) \right),$$

654 where $p(\mathbf{x}_1, \dots, \mathbf{x}_m)$ is defined in (6.2). By comparing (6.3) and (6.2) we conclude,
 655 up to terms of $\mathcal{O}(\nu^2)$, that the trap configurations that provide local minima for the
 656 average MFPT also provide local maxima for the first Neumann eigenvalue for (6.1).
 657 Qualitatively, this implies that, up to terms of order $\mathcal{O}(\nu^2)$, the trap configuration
 658 that maximizes the rate at which a Brownian particle is captured also provides the
 659 best configuration to minimize the average mean first capture time of the particle.
 660 In this way, our optimal trap configurations for the average MFPT for the ellipse
 661 identified in § 4.1 also correspond to trap patterns that maximize λ_0 up to terms of
 662 order $\mathcal{O}(\nu^2)$. Moreover, we remark that for the special case of a ring-pattern of traps,
 663 the first two-terms in (6.3) provide an exact solution of (4.1). As such, for these
 664 special patterns, the trap configuration that maximizes the $\mathcal{O}(\nu^2)$ term in λ_0 provides
 665 the optimal trap locations that minimize the average MFPT to *all orders in ν* .

666 Finally, we discuss two possible extensions of this study. Firstly, in near-disk do-
 667 mains and in the ellipse it would be worthwhile to use a more refined gradient descent
 668 procedure such as in [22] and [5] to numerically identify globally optimum trap con-
 669 figurations for a much larger number of identical traps than considered herein. One
 670 key challenge in upscaling the optimization procedure to a larger number of traps is
 671 that the energy landscape can be rather flat or else have many local minima, and
 672 so identifying the true optimum pattern is delicate. Locally optimum trap patterns
 673 with very similar minimum values for the average MFPT already occurs in certain
 674 near-disk domains at a rather small number of traps (see Fig. 1 and Fig. 4). One
 675 advantage of our asymptotic theory leading to (2.26) for the near-disk and (4.1) for
 676 the ellipse, is that it can be implemented numerically with very high precision. As
 677 a result, small differences in the average MFPT between two distinct locally opti-
 678 mal trap patterns are not due to discretization errors arising from either numerical

679 quadratures or evaluations of the Neumann Green's function. As such, combining our
 680 hybrid theory with a refined global optimization procedure should lead to the reliable
 681 identification of globally optimal trap configurations for these domains.

682 Another open direction is to investigate whether there are computationally useful
 683 analytical representations for the Neumann Green's function in an arbitrary bounded
 684 2-D domain. In this direction, in [13, Theorem 4.1] an explicit analytical result for the
 685 gradient of the regular part of the Neumann Green's function was derived in terms of
 686 the mapping function for a general class of mappings of the unit disk. It is worthwhile
 687 to study whether this analysis can be extended to provide a simple and accurate
 688 approach to compute the Neumann Green's matrix for an arbitrary domain. This
 689 matrix could then be used in the linear algebraic system (4.1) to calculate the average
 690 MFPT, and a gradient descent scheme implemented to identify optimal patterns.

691 **7. Acknowledgements.** Colin Macdonald and Michael Ward were supported
 692 by NSERC Discovery grants. Tony Wong was partially supported by a UBC Four-
 693 Year Graduate Fellowship.

694 **Appendix A. Derivation of the Thin Domain ODE.** In the asymptotic
 695 limit of a long thin domain, we use a perturbation approach on the MFPT PDE (2.2)
 696 for $u(x, y)$ in order to derive the limiting problem (4.8). We introduce the stretched
 697 variables X and Y by $X = \delta x, Y = y/\delta$ and $d = x_0/\delta$, and set $U(X, Y) = u(X/\delta, Y\delta)$.
 698 Then the PDE in (2.2) becomes $\delta^4 \partial_{XX} U + \partial_{YY} U = -\delta^2/D$. By expanding $U =$
 699 $\delta^{-2}U_0 + U_1 + \delta^2U_2 + \dots$ in this PDE, we collect powers of δ to get

(A.1)

$$700 \quad \mathcal{O}(\delta^{-2}) : \partial_{YY}U_0 = 0; \quad \mathcal{O}(1) : \partial_{YY}U_1 = 0; \quad \mathcal{O}(\delta^2) : \partial_{YY}U_2 = -\frac{1}{D} - \partial_{XX}U_0.$$

701 On the boundary $y = \pm\delta F(\delta x)$, or equivalently $Y = \pm F(X)$, where $F(X) =$
 702 $\sqrt{1 - X^2}$, the unit outward normal is $\hat{\mathbf{n}} = \mathbf{n}/|\mathbf{n}|$, where $\mathbf{n} \equiv (-\delta^2 F'(X), \pm 1)$. The
 703 condition for the vanishing of the outward normal derivative in (2.2) becomes

$$704 \quad \partial_n u = \hat{\mathbf{n}} \cdot (\partial_x u, \partial_y u) = \frac{1}{|\mathbf{n}|} (-\delta^2 F', \pm 1) \cdot (\delta \partial_X U, \delta^{-1} \partial_Y U) = 0, \quad \text{on } Y = \pm F(X).$$

705 This is equivalent to the condition that $\partial_Y U = \pm \delta^4 F'(X) \partial_X U$ on $Y = \pm F(X)$. Upon
 706 substituting $U = \delta^{-2}U_0 + U_1 + \delta^2U_2 + \dots$ into this expression, and equating powers
 707 of δ , we obtain on $Y = \pm F(X)$ that

$$708 \quad (\text{A.2}) \quad \mathcal{O}(\delta^{-2}) : \partial_Y U_0 = 0; \quad \mathcal{O}(1); \quad \partial_Y U_1 = 0; \quad \mathcal{O}(\delta^2); \quad \partial_Y U_2 = \pm F'(X) \partial_X U_0.$$

709 From (A.1) and (A.2) we conclude that $U_0 = U_0(X)$ and $U_1 = U_1(X)$. Assuming that
 710 the trap radius ε is comparable to the domain width δ , we will approximate the zero
 711 Dirichlet boundary condition on the three traps as zero point constraints for U_0 .

712 The ODE for $U_0(X)$ is derived from a solvability condition on the $\mathcal{O}(\delta^2)$ problem:
 (A.3)

$$713 \quad \partial_{YY}U_2 = -\frac{1}{D} - U_0'', \quad \text{in } \Omega \setminus \Omega_a; \quad \partial_Y U_2 = \pm F'(X) U_0', \quad \text{on } Y = \pm F(X), \quad |X| < 1.$$

714 We multiply this problem for U_2 by U_0 and integrate in Y over $|Y| < F(X)$. Upon

715 using Lagrange's identity and the boundary conditions in (A.3) we get

$$(A.4) \quad \int_{-F(X)}^{F(X)} (U_0 \partial_{YY} U_2 - U_2 \partial_{YY} U_0) dY = [U_0 \partial_Y U_2 - U_2 \partial_Y U_0] \Big|_{-F(X)}^{F(X)} = 2U_0 F'(X) U_0',$$

$$716 \quad \int_{-F(X)}^{F(X)} U_0 \left(-\frac{1}{D} - U_0'' \right) dY = -2F(X) U_0 \left(\frac{1}{D} + U_0'' \right) = 2U_0 F'(X) U_0'.$$

717 Thus, $U_0(X)$ satisfies the ODE $[F(X)U_0']' = -F(X)/D$, with $F(X) = \sqrt{1-X^2}$, as
718 given in (4.8) of § 4.2. This gives the leading-order asymptotics $u \sim \delta^{-2} U_0(X)$.

719 **Appendix B. Limiting Case of the Unit Disk.** We now show how to recover
720 the well-known Neumann Green's function and its regular part for the unit disk by
721 letting $a \rightarrow b = 1$ in (4.5) and (4.6), respectively. In the limit $\beta \equiv (a-b)/(a+b) \rightarrow 0$
722 only the $n = 0$ terms in the infinite sums in (4.5) and (4.6) are non-vanishing. In
723 addition, as $\beta \rightarrow 0$, we obtain from (4.3) that $|\mathbf{x}|^2 \sim f^2 e^{2\xi}/4$ and $|\mathbf{x}_0|^2 \sim f^2 e^{2\xi_0}/4$,
724 and $\xi_b = -\log f + \log(a+b) \rightarrow -\log f + \log 2$, where $f \equiv \sqrt{a^2 - b^2}$. This yields that

$$725 \quad (B.1) \quad \xi + \xi_0 - 2\xi_b \sim \log \left(\frac{2|\mathbf{x}|}{f} \right) + \log \left(\frac{2|\mathbf{x}_0|}{f} \right) - 2 \log 2 + 2 \log f = \log (|\mathbf{x}||\mathbf{x}_0|).$$

726 As such, only the z_1 and z_4 terms in the infinite sums in (4.5a) with $n = 0$ persist as
727 $a \rightarrow b = 1$, and so (4.5a) reduces in this limit to

(B.2)

$$728 \quad G(\mathbf{x}; \mathbf{x}_0) \sim \frac{1}{4|\Omega|} (|\mathbf{x}|^2 + |\mathbf{x}_0|^2) - \frac{3}{8|\Omega|} + \frac{1}{2\pi} (\xi_b - \xi_>) - \frac{1}{2\pi} \log |1 - z_1| - \frac{1}{2\pi} \log |1 - z_4|,$$

729 where $|\Omega| = \pi$ and $\xi_> \equiv \max(\xi_0, \xi)$. Since $\eta \rightarrow \theta$ and $\eta_0 \rightarrow \theta_0$, where θ and θ_0 are the
730 polar angles for \mathbf{x} and \mathbf{x}_0 , we get from (4.5b) that $z_4 \rightarrow |\mathbf{x}||\mathbf{x}_0| e^{i(\theta - \theta_0)}$ as $a \rightarrow b = 1$.

731 We then calculate that

(B.3)

$$732 \quad -\frac{1}{2\pi} \log |1 - z_4| = -\frac{1}{4\pi} \log |1 - z_4|^2 = -\frac{1}{4\pi} \log (1 - 2|\mathbf{x}||\mathbf{x}_0| \cos(\theta - \theta_0) + |\mathbf{x}|^2 |\mathbf{x}_0|^2).$$

733 Next, with regards to the z_1 term we calculate for $a \rightarrow b = 1$ that

$$734 \quad (B.4) \quad |\xi - \xi_0| = \begin{cases} \xi - \xi_0 \sim \log \left(\frac{|\mathbf{x}|}{|\mathbf{x}_0|} \right), & \text{if } 0 < |\mathbf{x}_0| < |\mathbf{x}|, \\ -(\xi - \xi_0) \sim \log \left(\frac{|\mathbf{x}_0|}{|\mathbf{x}|} \right), & \text{if } 0 < |\mathbf{x}| < |\mathbf{x}_0|. \end{cases}$$

735 From (4.5b) this yields for $a \rightarrow b = 1$ that

$$736 \quad (B.5) \quad z_1 = e^{-|\xi - \xi_0| + i(\eta - \eta_0)} \sim \begin{cases} \frac{|\mathbf{x}_0|}{|\mathbf{x}|} e^{i(\theta - \theta_0)}, & \text{if } 0 < |\mathbf{x}_0| < |\mathbf{x}|, \\ \frac{|\mathbf{x}|}{|\mathbf{x}_0|} e^{i(\theta - \theta_0)}, & \text{if } 0 < |\mathbf{x}| < |\mathbf{x}_0|. \end{cases}$$

737 By using (B.5), we calculate for $a \rightarrow b = 1$ that

$$738 \quad (B.6) \quad -\frac{1}{4\pi} \log |1 - z_1|^2 = -\frac{1}{2\pi} \log |\mathbf{x} - \mathbf{x}_0| + \begin{cases} \frac{1}{4\pi} \log |\mathbf{x}|^2, & \text{if } 0 < |\mathbf{x}_0| < |\mathbf{x}|, \\ \frac{1}{4\pi} \log |\mathbf{x}_0|^2, & \text{if } 0 < |\mathbf{x}| < |\mathbf{x}_0|. \end{cases}$$

739 Next, we estimate the remaining term in (B.2) as $a \rightarrow b = 1$ using

$$740 \quad (B.7) \quad \frac{1}{2\pi} (\xi_b - \xi_>) = \frac{1}{2\pi} \begin{cases} \xi_b - \xi \sim -\frac{1}{2\pi} \log |\mathbf{x}|, & \text{if } |\mathbf{x}| > |\mathbf{x}_0| > 0, \\ \xi_b - \xi_0 \sim -\frac{1}{2\pi} \log |\mathbf{x}_0|, & \text{if } 0 < |\mathbf{x}| < |\mathbf{x}_0|. \end{cases}$$

741 Finally, by using (B.3), (B.6), and (B.7) into (B.2), we obtain for $a \rightarrow b = 1$ that

$$742 \quad (B.8) \quad G(\mathbf{x}; \mathbf{x}_0) \sim -\frac{1}{2\pi} \log |\mathbf{x} - \mathbf{x}_0| - \frac{1}{4\pi} \log (1 - 2|\mathbf{x}||\mathbf{x}_0| \cos(\theta - \theta_0) + |\mathbf{x}|^2 |\mathbf{x}_0|^2) \\ + \frac{1}{4|\Omega|} (|\mathbf{x}|^2 + |\mathbf{x}_0|^2) - \frac{3}{8|\Omega|},$$

743 where $|\Omega| = \pi$. This result agrees with that in (3.1a) for the Neumann Green's
744 function in the unit disk. Similarly, we can show that the regular part R_e for the
745 ellipse given in (4.6) tends as $a \rightarrow b = 1$ to that given in (3.1b) for the unit disk.

746 Appendix C. Asymptotics of the Fundamental Neumann Eigenvalue.

747 For $\nu \ll 1$, it was shown in [12], by using a matched asymptotic expansion analysis
748 in the limit of small trap radii similar to that leading to (4.1), that the fundamental
749 Neumann eigenvalue λ_0 for (6.1) is the smallest positive root of

$$750 \quad (C.1) \quad \mathcal{K}(\lambda) \equiv \det(I + 2\pi\nu\mathcal{G}_H) = 0.$$

751 Here $\nu = -1/\log \varepsilon$ and \mathcal{G}_H is the Helmholtz Green's matrix with matrix entries

$$752 \quad (C.2) \quad (\mathcal{G})_{Hjj} = R_{Hj} \text{ for } i = j \text{ and } (\mathcal{G})_{Hij} = (\mathcal{G})_{Hji} = G_H(\mathbf{x}_i; \mathbf{x}_j) \text{ for } i \neq j,$$

754 where the Helmholtz Green's function $G_H(\mathbf{x}; \mathbf{x}_j)$ and its regular part R_{Hj} satisfy

$$755 \quad (C.3a) \quad \Delta G_H + \lambda G_H = -\delta(\mathbf{x} - \mathbf{x}_j), \quad \mathbf{x} \in \Omega; \quad \partial_n G_H = 0, \quad \mathbf{x} \in \partial\Omega;$$

$$756 \quad (C.3b) \quad G_H \sim -\frac{1}{2\pi} \log |\mathbf{x} - \mathbf{x}_j| + R_{Hj} + o(1), \quad \text{as } \mathbf{x} \rightarrow \mathbf{x}_j.$$

758 For $0 < \lambda \ll 1$, we estimate \mathcal{G}_H by expanding $G_H = A/\lambda + G + \mathcal{O}(\lambda)$, for some A to
759 be found. From (C.3), we derive in terms of the Neumann Green's matrix \mathcal{G} that

$$760 \quad (C.4) \quad \mathcal{G}_H = -\frac{m}{\lambda|\Omega|} E + \mathcal{G} + \mathcal{O}(\lambda), \quad \text{with } E \equiv \frac{1}{m} \mathbf{e}\mathbf{e}^T,$$

761 for $0 < \lambda \ll 1$. From (C.4) and (C.1), the fundamental Neumann eigenvalue λ_0 is the
762 smallest $\lambda > 0$ for which there is a nontrivial solution $\mathbf{c} \neq \mathbf{0}$ to

$$763 \quad (C.5) \quad \left(I - \frac{2\pi\nu m}{\lambda|\Omega|} E + 2\pi\nu\mathcal{G} + \mathcal{O}(\nu) \right) \mathbf{c} = 0.$$

764 Since this occurs when $\lambda = \mathcal{O}(\nu)$, we define $\lambda_c > 0$ by $\lambda = 2\pi\nu m \lambda_c / |\Omega|$, so that (C.5)
765 can be written in equivalent form as

$$766 \quad (C.6) \quad E\mathbf{c} = \lambda_c (I + 2\pi\nu\mathcal{G} + \mathcal{O}(\nu^2)) \mathbf{c}, \quad \text{where } \lambda = \frac{2\pi\nu m}{|\Omega|} \lambda_c.$$

767 Since $E\mathbf{e} = \mathbf{e}$, while $E\mathbf{q} = 0$ for any $\mathbf{q} \in \mathbb{R}^{m-1}$ with $\mathbf{e}^T \mathbf{q} = 0$, we conclude for $\nu \ll$
768 1 that the only non-zero eigenvalue of (C.6) satisfies $\lambda_c \sim 1$ with $\mathbf{c} \sim \mathbf{e}$. To determine
769 the correction to this leading-order result, in (C.6) we expand $\lambda_c = 1 + \nu\lambda_{c1} + \dots$
770 and $\mathbf{c} = \mathbf{e} + \nu\mathbf{c}_1 + \dots$. From collecting $\mathcal{O}(\nu)$ terms in (C.6), we get

$$771 \quad (C.7) \quad (I - E)\mathbf{c}_1 = -2\pi\mathcal{G}\mathbf{e} - \lambda_{c1}\mathbf{e}.$$

772 Since $I - E$ is symmetric with the 1-D nullspace \mathbf{e} , the solvability condition for (C.7)
773 is that $-2\pi\mathbf{e}^T \mathcal{G}\mathbf{e} - \lambda_{c1}\mathbf{e}^T \mathbf{e} = 0$. Since $\mathbf{e}^T \mathbf{e} = m$, this yields the two-term expansion

$$774 \quad (C.8) \quad \lambda_c = 1 + \nu\lambda_{c1} + \dots, \quad \text{where } \lambda_{c1} = -\frac{2\pi}{m} \mathbf{e}^T \mathcal{G}\mathbf{e}.$$

775 Finally, using $\lambda = 2\pi\nu m \lambda_c / |\Omega|$, we obtain the two-term expansion as given in (6.2).

776

REFERENCES

- 777 [1] O. Bénichou and R. Voituriez. From first-passage times of random walks in confinement to
778 geometry-controlled kinetics. *Physics Reports*, 539(4):225–284, 2014.
- 779 [2] P. Bressloff and S. D. Lawley. Stochastically gated diffusion-limited reactions for a small target
780 in a bounded domain. *Phys. Rev. E.*, 92:062117, 2015.
- 781 [3] A. F Cheviakov, M. J Ward, and R. Straube. An asymptotic analysis of the mean first passage
782 time for narrow escape problems: Part II: The sphere. *SIAM J. Multiscale Model. Simul.*,
783 8(3), 2010.
- 784 [4] D. Coombs, R. Straube, and M. J. Ward. Diffusion on a sphere with localized traps: Mean
785 first passage time, eigenvalue asymptotics, and Fekete points. *SIAM J. Appl. Math.*, 70(1),
786 2009.
- 787 [5] J. Gilbert and A. Cheviakov. Globally optimal volume-trap arrangements for the narrow-
788 capture problem inside a unit sphere. *Phys. Rev. E.*, 99(012109), 2019.
- 789 [6] I. V Grigoriev, Y. A Makhnovskii, A. M Berezhkovskii, and V. Yu Zitserman. Kinetics of
790 escape through a small hole. *J. Chem. Phys.*, 116(22):9574–9577, 2002.
- 791 [7] D. Holcman and Z. Schuss. Escape through a small opening: receptor trafficking in a synaptic
792 membrane. *J. Stat. Phys.*, 117(5-6):975–1014, 2004.
- 793 [8] D. Holcman and Z. Schuss. The narrow escape problem. *SIAM Review*, 56(2):213–257, 2014.
- 794 [9] D. Holcman and Z. Schuss. Time scale of diffusion in molecular and cellular biology. *J. of*
795 *Physics A: Math. and Theor.*, 47(17):173001, 2014.
- 796 [10] S. Iyaniwura, T. Wong, M. J. Ward, and C. B. Macdonald. Simulation and optimization of mean
797 first passage time problems in 2-d using numerical embedded methods and perturbation
798 theory. *submitted, SIAM J. Multiscale Model. Simul.*, 2019.
- 799 [11] J. Kennedy. Particle swarm optimization. *Encyclopedia of machine learning*, pages 760–766,
800 2010.
- 801 [12] T. Kolokolnikov, M. S Titcombe, and M. J. Ward. Optimizing the fundamental Neumann eigen-
802 value for the Laplacian in a domain with small traps. *Europ. J. Appl. Math.*, 16(2):161–200,
803 2005.
- 804 [13] T. Kolokolnikov and M. J. Ward. Reduced wave Green’s functions and their effect on the
805 dynamics of a spike for the Gierer-Meinhardt model. *Europ. J. Appl. Math*, 14(5):513–545,
806 2003.
- 807 [14] T. Kolokolnikov, M. J. Ward, and J. Wei. Spot self-replication and dynamics for the Schnaken-
808 burg model in a two-dimensional domain. *J. Nonl. Science*, 19(1):1–56, 2009.
- 809 [15] V. Kurella, J. C Tzou, D. Coombs, and M. J Ward. Asymptotic analysis of first passage time
810 problems inspired by ecology. *Bull. Math. Biol.*, 77(1), 2015.
- 811 [16] A. E. Lindsay, A. J. Bernoff, and M. J. Ward. First passage statistics for the capture of a
812 Brownian particle by a structured spherical target with multiple surface traps. *SIAM J.*
813 *Multiscale Model. Simul.*, 15(1):74–109, 2017.
- 814 [17] S. L. Marshall. A rapidly convergent modified Green’s function for Laplace’s equation in a
815 rectangular domain. *Proc. Roy. Soc. London A*, 455:1739–1766, 1999.
- 816 [18] R. C. McCann, R. D. Hazlett, and D. K. Babu. Highly accurate approximations of Green’s and
817 Neumann functions on rectangular domains. *Proc. Roy. Soc. Lond. A*, 457:767–772, 2001.
- 818 [19] S. Pillay, M. J Ward, A. Peirce, and T. Kolokolnikov. An asymptotic analysis of the mean
819 first passage time for narrow escape problems: Part I: Two-dimensional domains. *SIAM*
820 *J. Multiscale Model. Simul.*, 8(3), 2010.
- 821 [20] S. Redner. *A guide to first-passage processes*. Cambridge University Press, 2001.
- 822 [21] L. M Ricciardi. Diffusion approximations and first passage time problems in population biology
823 and neurobiology. In *Mathematics in Biology and Medicine*, pages 455–468. Springer, 1985.
- 824 [22] W. J. M. Ridgway and A. Cheviakov. Locally and globally optimal configurations of n particles
825 on the sphere with applications in the narrow escape and narrow capture problems. *Phys.*
826 *Rev. E.*, 100(042413), 2019.
- 827 [23] Z. Schuss, A. Singer, and D. Holcman. The narrow escape problem for diffusion in cellular
828 microdomains. *Proc. Natl. Acad. Sci.*, 104(41):16098–16103, 2007.
- 829 [24] A. Singer, Z. Schuss, and D. Holcman. Narrow escape, Part II: The circular disk. *J. Stat.*
830 *Phys.*, 122(3):465–489, 2006.
- 831 [25] L. N. Trefethen and J. A. C. Weideman. The exponentially convergent trapezoidal rule. *SIAM*
832 *Review*, 56(3):28–51, 2014.
- 833 [26] M. J. Ward, W. D. Henshaw, and J. B. Keller. Summing logarithmic expansions for singularly
834 perturbed eigenvalue problems. *SIAM J. Appl. Math.*, 53(3):799–828, 1993.
- 835 [27] M. J. Ward and J. B. Keller. Strong localized perturbations of eigenvalue problems. *SIAM J.*
836 *App. Math.*, 53(3):770–798, 1993.